ICARUS 100, 162–186 (1992)

0.7- to 23-μm Photometric Observations of P/Halley 1986 III and Six Recent Bright Comets

R. D. GEHRZ AND E. P. NEY

Astronomy Department, School of Physics and Astronomy, 116 Church Street S.E., University of Minnesota, Minneapolis, Minnesota 55455

Received March 30, 1992; revised July 23, 1992

We report 0.7- to 23-μm observations of P/Halley 1986 III and six other recent bright comets. P/Halley was measured on 47 occasions between 1985 December 12 UT and 1986 May 6 UT, several times within hours of the perihelion passage on 1986 February 9 UT. Our data show that the strength of the 10-μm silicate emission feature and the temperature excess (superheat; $S = T_{obs}/T_{BB}$) of the infrared continuum emission are strongly correlated. IR Type I comets have low continuum superheat and muted or undetectable silicate emission features, suggesting that the coma emission from these comets is produced by large grains with radii larger than 1 μm. IR Type II comets have superheated thermal infrared continua and high-contrast silicate emission features, indicating that the coma emission is from small grains with radii between 0.5 and 1 μm. Both types of behavior were exhibited by Comet P/Halley at various times. The relationship between superheat and 10-μm silicate emission may be complex, for although the strength of these quantities was generally strongly correlated, several comets exhibited occasional episodes when superheat and silicate emission were not correlated. P/Halley's dust coma had an average albedo of 0.20 at a scattering angle of 130°. Our data show that the scattering phase function for typical comet dust is characterized by a moderately strong forward scattering peak, no appreciable backscattering peak, a mean bolometric albedo of $\approx$0.32, and an albedo of $\approx$0.15 for scattering angles between 120° and 180°. These characteristics are consistent with laboratory and theoretical results for nonspherical and "fluffy" core–mantle aggregate grains. P/Halley's 10-μm silicate signature showed significant variations in strength and was occasionally weak or absent at heliocentric distances both smaller and larger than 1 AU. Simultaneous measurements of P/Halley and Bradfield 1980 XV with different diaphragms are generally consistent with the steady-state model for nuclear ablation. P/Halley's coma luminosity fluctuated by a factor of nearly 10 on time scales of 1 to 2 days. These variations are consistent with jet-like activity probably associated with nuclear rotation. Dust mass loss rates for the comets studied here are estimated, and we conclude that P/Halley was losing $\geq 10^6$ g sec^{-1} of dust at a heliocentric distance of 1 AU.

I. INTRODUCTION

Infrared observations of comets can yield fundamental information about the composition and structure of astrophysical dust grains. Comet nuclei are believed to contain samples of the primary solid and condensible constituents of the primitive Solar System frozen in the state in which they were trapped during the epoch of comet nucleus formation. During perihelion passage, this primordial material can be studied by modern-day observers as the nucleus is ablated by sunlight to form the coma and tail. More than 20 years ago, observations of Comet Ikeya-Seki by Becklin and Westphal (1966) first showed that comets are strong infrared sources because of thermal emission from dust grains that are driven away from the nucleus by the evaporation of volatiles such as water and carbon dioxide ices. We subsequently observed many bright comets to define the properties of cometary grains and study the characteristics of the ablation of comet nuclei (Maas *et al.* 1970, Ney 1974a, 1974b, 1982a, Gehrz *et al.* 1989, and Hanner *et al.* 1990). Our investigations were based on measurements of the reflected and thermally reradiated energy from grains in comet comae, tails, and the antitail of Comet Kohoutek. Comets are especially important because they present the only case in which the light scattering phase function of astrophysical grains can be determined with reasonable certainty. Their heliocentric and geocentric distances, and hence their scattering angles, can be determined.

In this paper, we present 0.7- to 23-μm infrared photometry of P/Halley 1986 III and six other recent bright comets, and we discuss the data in the context of our previous infrared studies of comets.

II. THE OBSERVATIONS

We used broadband optical/infrared photometers that measure from 0.7 to 23 micrometers mounted on the University of Minnesota (UM1, UM2) O'Brien 0.76-m telescope, the Wyoming Infrared Observatory (WIRO) 2.34-m telescope, and the UM Mount Lemmon Observing Facility (MLOF) 1.52-m telescope to measure Comet P/Halley 47 times between 1985 December 12 UT and 1986 May 6 UT. Data for six other recent bright comets that we observed near perihelion passage are presented

0019-1035/92 $5.00

here for comparison. These were Comets Kobayashi–Berger–Milon 1975 IX (KBM), Bradfield 1980 XV (1980t), Austin 1984 XIII (1984i), Machholz 1985 VIII (1985e), Austin 1989c$_1$ (designated 1990 V after this paper went to press), and Brorson–Metcalf 1989 X (BM). The photometric results and important parameters related to the analysis presented below are summarized in Tables I–IV, and Appendix C (Table C-I). The photometric systems, magnitude scales, and absolute flux calibrations for the UM and MLOF measurements were described by Ney (1974a). Gehrz *et al.* (1974, 1987) described these parameters for the photometric system used at WIRO. Comments on a preliminary reduction of a subset of the P/Halley data were presented by Gehrz and Ney (1986). Ney (1982a) discussed the initial analysis of the data on Comets KBM and Bradfield 1980 XV. On three occasions, simultaneous measurements were obtained with the UM and WIRO telescopes using different beam diameters. The O'Brien and WIRO telescopes were the *only* infrared telescopes in the world that monitored P/Halley from mid January to late February 1986 III during its perihelion passage.

Nearly all the measurements made at WIRO were obtained using a telephone observing link enabling us to control the computer-operated Wyoming Infrared Telescope (Gehrz and Hackwell 1978) remotely from the University of Minnesota. All data acquisition parameters and telescope control functions were commanded by the remote observer over two 2400-Baud telephone lines, and a third telephone line was used to communicate with an on-site assistant whose main task was to center offset guide stars on a reticle upon request. A continuous stripchart of the infrared-detector output enabled the remote observer to center sources in the photometer beam and monitor data acquisition. Automatic searching and peaking routines were used to find bright objects and to keep them centered. This system is, to our knowledge, the first substantial demonstration of the routine use of remote control to obtain data from a groundbased optical/infrared telescope.

Data in Table II are raw magnitudes corrected only for atmospheric extinction. These data are uncorrected for the contribution of the coma emission in the reference beam. Since the coma is extended, the beam-switching technique we employed in taking our data automatically subtracts the coma emission in the reference beam from the coma emission in the source beam. Correction factors which must be applied to reconstruct the full signal that would have been observed in the source beam if the reference beam had been placed off the coma depend on the surface brightness distribution of the coma. The correction factors used in the quantitative analysis described below are derived in detail in Appendixes A and B and are supplied in Tables I and III. Several of the photometers had square diaphragms as noted in the footnotes to Tables I and II. We derived the equivalent circular aperture diameters cited in Table I (column 12) and Table II (column 6) by comparing the integrated fluxes that would be observed in circular and square diaphragms using the r^{-1} coma surface brightness distribution given by the steady-state model described in Appendix A.

All three tables contain five identical leading columns that serve to characterize the observations on each date: column 1, a chronological observation number; 2, the UT observation date; 3, the Julian date of the observation; 4, the UT time of each observation in decimal days with respect to perihelion passage ($t = 0$) where negative and positive values indicate pre- and postperihelion observations, respectively; and 5, the photometric system in use at the time of each observation. The remaining columns in Table I give the physical parameters of the comet orbit computed using the orbital elements given in Appendix C, the photometer configuration, and the correction factors required to normalize the observations: 6, the heliocentric distance r in AU; 7, the geocentric distance Δ in AU; 8, the multiplier to correct the observed coma emission to $r = 1$ and $\Delta = 1$; 9, the elongation (Sun–Earth–comet) angle θ_{el}; 10, the scattering (Sun–comet–Earth) angle θ, (11), the phase angle θ_{ph} ($\theta_{ph} = 180° - \theta$); 12, the beam diameter ϕ in arcseconds (the equivalent circular diameter is given for photometers with square beams); 13, the chopper throw ψ between the source and reference beams in arcseconds; 14, the multiplier required to correct for coma emission in the reference beam; 15, the multiplier to normalize the coma emission to a circular diaphragm of 20-arcsec diameter; and 16, the multiplier that gives the coma emission in a standard beam of diameter 20 arcsec corrected for emission into the reference beam. The remaining columns in Table II give: 6, the diaphragm diameter ϕ in arcseconds (the equivalent circular diameter is given for photometers with square beams); 7, the chopper throw ψ between the source and the reference beams in arcseconds, and columns 8 through 21, the raw photometric magnitudes corrected only for atmospheric extinction. The remaining columns in Table III summarize physical quantities derived from the data given in Table II, orbital parameters computed using the orbital elements given in Appendix C (Table C-I), and the correction factors derived in Appendixes A and B: 6, r; 7, Δ; 8, the temperature T_{BB} of a black conducting sphere at heliocentric distance r; 9, the measured infrared color temperature T_{obs} of the comet's continuum emission; 10, the superheat S of the continuum emission; 11, the observed apparent maximum emission from the infrared continuum $[\lambda f_\lambda(\mathrm{IR})]_{max}$ in W cm^{-2}; 12, the observed apparent maximum emission from the scattered solar component $[\lambda f_\lambda(V)]_{max}$ in W cm^{-2}; 13, the albedo $A(\theta)$ of the coma at the scattering angle θ from Eq. (6); 14, the equivalent blackbody angular

TABLE I
Optical and Observational Parameters for Comet P/Halley and Six Other Bright Comets

(1)	(2)	(3)	(4)	(5)	(6)	(7)	(8)	(9)	(10)	(11)	(12)	(13)	(14)	(15)	(16)
#	UT DATE	JD 2,440,000+	Days from Perihelion	SYSTEM	r AU	Δ AU	$\frac{1}{r^4\Delta}$	θ_{el} deg	θ deg	θ_{ph} deg	φ arcsec^1	ψ arcsec	$\frac{4\psi}{4\psi-\phi}$	$\frac{20}{\phi}$	$[\frac{4\psi}{4\psi-\phi}][\frac{20}{\phi}]$
Comet P/Halley 1986 III															
1	12.11 Dec, 1985	6411.61	-59.35	UM2	1.32	0.77	0.43	97	132	48	22.5	30	1.23	0.89	1.09
2	13.06 Dec, 1985	6412.56	-58.40	UM2	1.30	0.79	0.44	94	131	49	22.5	30	1.23	0.89	1.09
3	14.01 Dec, 1985	6413.51	-57.45	UM2	1.29	0.80	0.45	92	130	50	22.5	30	1.23	0.89	1.09
4	25.00 Dec, 1985	6424.50	-46.46	UM2	1.11	1.02	0.65	68	125	55	22.5	30	1.23	0.89	1.09
5	30.00 Dec, 1985	6429.50	-41.46	UM2	1.04	1.12	0.76	59	126	54	22.5	30	1.23	0.89	1.09
6	1.01 Jan, 1986	6431.51	-39.45	UM2	1.01	1.16	0.83	56	127	53	22.5	30	1.23	0.89	1.09
7	7.89 Jan, 1986	6438.39	-32.57	UM2	0.90	1.29	1.18	44	130	50	22.5	30	1.23	0.89	1.09
8	11.1 Jan, 1986	6441.60	-29.36	WIRO	0.86	1.34	1.36	40	133	47	5	16	1.08	4.00	4.32
9	11.9 Jan, 1986	6442.40	-28.56	WIRO	0.85	1.35	1.42	38	134	46	5	17	1.08	4.00	4.32
10	12.0 Jan, 1986	6442.50	-28.46	UM2	0.84	1.48	1.48	38	134	46	22.5	30	1.23	0.89	1.09
11	12.7 Jan, 1986	6443.20	-27.76	WIRO	0.84	1.36	1.48	40	135	45	5	18	1.07	4.00	4.28
12	12.7 Jan, 1986	6443.20	-27.76	WIRO	0.84	1.36	1.48	40	135	45	5	18	1.07	4.00	4.28
13	12.8 Jan, 1986	6443.30	-27.66	WIRO	0.84	1.36	1.48	40	135	45	2.2	18	1.03	9.09	9.36
14	12.8 Jan, 1986	6443.30	-27.66	WIRO	0.84	1.36	1.48	40	135	45	3.3	18	1.05	6.06	6.36
15	12.9 Jan, 1986	6443.40	-27.56	WIRO	0.84	1.36	1.48	40	135	45	8.3	18	1.13	2.41	2.72
16	26.8 Jan, 1986	6457.30	-13.60	UM2	0.66	1.54	3.42	17	154	26	22.5	30	1.23	0.89	1.09
17	9.75 Feb, 1986	6471.25	+00.29	UM2	0.59	1.54	5.36	8.5	166	14	22.5	30	1.23	0.89	1.09
18	9.83 Feb, 1986	6471.33	+00.37	WIRO	0.59	1.54	5.36	8.5	166	14	8.3	18	1.13	2.41	2.72
19	9.85 Feb, 1986	6471.35	+00.39	UM2	0.59	1.54	5.36	8.5	166	14	22.5	30	1.23	0.89	1.09
20	10.72 Feb, 1986	6472.22	+01.26	UM2	0.59	1.54	5.36	9.5	164	16	22.5	30	1.23	0.89	1.09
21	10.77 Feb, 1986	6472.27	+01.31	UM2	0.59	1.54	5.36	9.5	164	16	22.5	30	1.23	0.89	1.09
22	11.88 Feb, 1986	6473.38	+02.42	WIRO	0.59	1.53	5.39	11	162	18	8.3	20	1.12	2.41	2.70
23	12.67 Feb, 1986	6474.17	+03.21	UM2	0.59	1.52	5.43	12	160	20	22.5	30	1.23	0.89	1.09
24	12.74 Feb, 1986	6474.24	+03.28	UM2	0.59	1.52	5.43	12	160	20	22.5	30	1.23	0.89	1.09
25	14.67 Feb, 1986	6476.17	+05.21	UM2	0.60	1.50	5.14	15	156	24	22.5	30	1.23	0.89	1.09
26	14.79 Feb, 1986	6476.29	+05.33	UM2	0.60	1.50	5.14	15	156	24	22.5	30	1.23	0.89	1.09
27	21.7 Feb, 1986	6483.20	+12.24	UM2	0.65	1.40	4.00	24	141	39	22.5	30	1.23	0.89	1.09
28	27.69 Feb, 1986	6489.19	+18.23	UM2	0.71	1.30	3.03	33	130	50	22.5	30	1.23	0.89	1.09
29	27.70 Feb, 1986	6489.20	+18.24	WIRO	0.71	1.29	3.05	33	130	50	8.3	17.5	1.13	2.41	2.72
30	27.75 Feb, 1986	6489.25	+18.29	UM2	0.71	1.29	3.05	33	130	50	22.5	30	1.23	0.89	1.09
31	2.71 Mar, 1986	6492.21	+21.25	WIRO	0.75	1.22	2.59	37	126	54	5	5	1.33	4.00	5.32
32	2.71 Mar, 1986	6492.21	+21.25	WIRO	0.75	1.22	2.59	37	126	54	5	43	1.03	4.00	4.12
33	4.64 Mar, 1986	6494.14	+23.18	UM2	0.76	1.20	2.50	40	125	55	22.5	30	1.23	0.89	1.09
34	6.74 Mar, 1986	6496.24	+25.28	WIRO	0.80	1.13	2.16	43	122	58	5	40	1.03	4.00	4.12
35	7.61 Mar, 1986	6497.11	+26.15	UM2	0.81	1.12	2.17	45	120	60	22.5	30	1.23	0.89	1.09
36	13.62 Mar, 1986	6503.12	+32.16	WIRO	0.90	0.97	1.57	54	116	64	5	5	1.33	4.00	5.32
37	13.62 Mar, 1986	6503.12	+32.16	WIRO	0.90	0.97	1.57	54	116	64	5	20	1.07	4.00	4.28
38	15.63 Mar, 1986	6505.13	+34.17	UM2	0.92	0.92	1.50	58	115	65	22.5	30	1.23	0.89	1.09
39	20.58 Mar, 1986	6510.08	+39.12	UM2	1.00	0.80	1.25	67	114	66	22.5	30	1.23	0.89	1.09
40	23.5 Mar, 1986	6513.00	+42.04	UM2	1.05	0.72	1.14	73	115	65	22.5	30	1.23	0.89	1.09
41	25.5 Mar, 1986	6515.00	+44.04	MLOF	1.08	0.68	1.08	76	115	65	15.2	23	1.20	1.32	1.58
42	28.55 Mar, 1986	6518.05	+47.09	WIRO	1.13	0.60	1.04	86	118	62	5	17	1.08	4.00	4.32
43	27.3 Apr, 1986	6547.80	+76.84	MLOF	1.57	0.69	0.24	81	153	27	10	20	1.14	2.00	2.28
44	28.3 Apr, 1986	6548.80	+77.84	MLOF	1.59	0.72	0.22	136	153	27	10	20	1.14	2.00	2.28
45	1.21 May, 1986	6551.71	+80.75	WIRO	1.63	0.80	0.18	129	151	29	5	20	1.07	4.00	4.28
46	5.2 May, 1986	6555.70	+84.74	UM2	1.69	0.92	0.13	122	150	30	22.5	30	1.23	0.89	1.09
47	6.2 May, 1986	6556.70	+85.74	UM2	1.71	0.96	0.12	121	149	31	22.5	30	1.23	0.89	1.09
COMET KOBAYASHI-BERGER-MILON 1975 IX															
1	27.7 July, 1975	2621.2	-39.6	UM1	1.02	0.32	2.89	82.5	100.1	79.9	30.3	30	1.34	0.66	0.88
2	27.7 Aug, 1975	2652.2	-08.6	UM1	0.48	0.99	19.0	27.9	101.0	79.0	30.3	30	1.34	0.66	0.88
3	31.9 Aug, 1975	2656.4	-04.4	UM1	0.44	1.09	24.5	24.0	111.8	68.2	30.3	30	1.34	0.66	0.88
4	1.9 Sep, 1975	2657.4	-03.4	UM1	0.44	1.11	24.0	23.2	114.3	65.7	30.3	30	1.34	0.66	0.88

TABLE I–*Continued*

(1)	(2)	(3)	(4)	(5)	(6)	(7)	(8)	(9)	(10)	(11)	(12)	(13)	(14)	(15)	(16)
#	UT DATE	JD 2,440,000+	Days from Perihelion	SYSTEM	r AU	Δ AU	$\frac{1}{r^4\Delta}$	θ_d deg	θ deg	θ_{ph} deg	φ arcsec[1]	ψ arcsec	$\frac{4\psi}{4\psi-\phi}$	$\frac{20}{\phi}$	$\left[\frac{4\psi}{4\psi-\phi}\right]\left[\frac{20}{\phi}\right]$
5	2.7 Sep, 1975	2658.2	-02.6	UM1	0.43	1.12	26.1	22.8	115.3	64.7	30.3	30	1.34	0.66	0.88
6	3.9 Sep, 1975	2659.4	-01.4	UM1	0.43	1.15	25.4	21.7	119.4	60.6	30.3	30	1.34	0.66	0.88
7	5.3 Sep, 1975	2660.8	-0.0	UM1	0.43	1.17	25.0	20.8	122.8	57.2	30.3	30	1.34	0.66	0.88
8	8.8 Sep, 1975	2664.3	+3.5	UM1	0.44	1.24	21.5	19.1	130.6	49.4	30.3	30	1.34	0.66	0.88
COMET BRADFIELD 1980 XV (1980t)															
1	1.8 Jan, 1981	4606.3	+03.3	UM2	0.28	0.73	222.9	8.4	30.6	149.3	22.5	30	1.23	0.89	1.09
2	2.8 Jan, 1981	4607.3	+4.3	UM2	0.30	0.75	164.6	11.8	42.7	137.3	22.5	30	1.23	0.89	1.09
3	3.8 Jan, 1981	4608.3	+5.3	UM2	0.31	0.77	140.6	14.9	53.7	126.3	22.5	30	1.23	0.89	1.09
4	9.7 Jan, 1981	4614.2	+11.2	UM2	0.44	0.96	27.8	26.2	99.7	80.3	22.5	30	1.23	0.89	1.09
5	11.9 Jan, 1981	4616.4	+13.4	UM2	0.49	1.04	16.7	28.0	110.4	69.6	22.5	30	1.23	0.89	1.09
6	16.8 Jan, 1981	4621.3	+18.3	UM2	0.61	1.23	5.9	29.5	127.3	52.7	22.5	30	1.23	0.89	1.09
7	17.9 Jan, 1981	4622.4	+19.4	UM2	0.64	1.27	4.7	29.6	130.1	49.9	22.5	30	1.23	0.89	1.09
8	18.8 Jan, 1981	4623.3	+20.3	UM2	0.66	1.30	4.1	29.5	132.4	47.6	22.5	30	1.23	0.89	1.09
9	21.8 Jan, 1981	4626.3	+23.3	UM2	0.72	1.41	2.6	29.0	138.7	41.3	22.5	30	1.23	0.89	1.09
10	22.9 Jan, 1981	4627.4	+24.4	WIRO	0.75	1.44	2.2	28.8	140.7	39.3	8.3	20	1.13	2.41	2.72
11	22.9 Jan, 1981	4627.4	+24.4	WIRO	0.75	1.44	2.2	28.8	140.7	39.3	5	20	1.07	4.00	4.28
12	24.8 Jan, 1981	4629.3	+26.3	UM2	0.79	1.51	1.7	28.4	143.8	36.2	22.5	30	1.23	0.89	1.09
COMET AUSTIN 1984 XIII (1984i)															
1	8.8 Aug, 1984	5921.3	-03.3	UM2	0.31	1.16	93.3	14.5	124.9	55.0	22.5	30	1.23	0.89	1.09
2	9.8 Aug, 1984	5922.3	-02.3	UM2	0.30	1.19	103.7	12.8	132.0	48.0	22.5	30	1.23	0.89	1.09
3	10.8 Aug, 1984	5923.3	-01.3	UM2	0.30	1.22	101.2	10.9	139.4	40.6	22.5	30	1.23	0.89	1.09
COMET MACHHOLZ 1985 VIII (1985e)															
1	24.75 Jun, 1985	6241.25	-4.0	UM2	0.22	1.09	391.6	11.2	115.9	64.1	22.5	30	1.23	0.89	1.09
COMET AUSTIN (1989c1)															
1	23.83 Mar, 1990	7974.33	-17.14	UM2	0.59	1.36	6.07	23.0	138.4	41.6	22.5	30	1.23	0.89	1.09
2	3.71 Apr, 1990	7985.21	-6.26	UM2	0.39	1.16	37.3	19.1	123.8	56.2	22.5	30	1.23	0.89	1.09
3	12.78 Apr, 1990	7994.28	+2.81	UM2	0.36	0.96	62.0	21.0	93.2	86.8	22.5	30	1.23	0.89	1.09
4	15.79 Apr, 1990	7997.29	+5.82	WIRO	0.39	0.88	49.1	22.7	83.8	96.2	5	50	1.03	4.00	4.12
COMET BRORSON-METCALF 1989 X (1989o)															
1	15.8 Sep, 1989	7785.3	+3.86	WIRO	0.49	1.23	14.10	22.5	127.9	52.1	5	27	1.04	4.00	4.22
2	16.7 Sep, 1989	7786.2	+4.76	WIRO	0.49	1.25	13.88	22.1	129.9	50.1	5	24	1.05	4.00	4.20

[1]Notes to Table 1:

UM1 had a 27" square beam which is equivalent to a 30.3" circular aperture;

UM2 had a 20" square beam which is equivalent to a 22.5" circular aperture; MLOF on 25 March, 1986 UT had a 13.5" square beam which is equivalent to a 15.2" circular aperture.

radius θ_r of the coma continuum in milliarcseconds; 15, the upper limit to radius of the nucleus, in kilometers, from the thermal emission maximum; 16 and 17, the correction factors (see Appendixes A and B) applied in reducing the photometric data to a common distance, beam diameter, and throw; and 18, the activity index as defined by the total infrared emission corrected for beam size, throw, and distance effects as described by Eqs. (11), (B-1), and (B-2). The quantities in columns 14 and 15 were calculated assuming that all the emission is from a nucleus that is point-like with respect to the beam (see Gehrz *et al.* 1989). In this case, the correction factors given by Eqs. (11), (B-1), and (B-2) do not apply.

III. DISCUSSION

The photometric data we report here for recent bright comets reveal some of the physical properties of the dust grains released by comet nuclei and help to define the nature of the nuclear ablation process.

TABLE II
Infrared Magnitudes for Comet P/Halley and Six Other Recent Bright Comets

(1)	(2)	(3)	(4)	(5)	(6)	(7)	(8)	(9)	(10)	(11)	(12)	(13)	(14)	(15)	(16)	(17)	(18)	(19)	(20)	(21)
#	UT DATE	JD 2,440,000+	Days from Perihelion	SYSTEM	ϕ arcsec	ψ arcsec	[0.7]	[1.2]	[1.6]	$[2.X]^2$	[3.6]	$[4.X]^2$	$[8.X]^2$	N	$[10.X]^2$	$[11.X]^2$	$[12.X]^2$	[18]	[19.5]	[23]
COMET P/HALLEY 1986 III																				
1	12.11 Dec, 1985	6411.61	-59.35	UM2	22.5	30	-	-	-	+6.8	+6.1	-	-0.5	-	-1.9	-	-1.9	-3.4	-	-
2	13.06 Dec, 1985	6412.56	-58.40	UM2	22.5	30	-	-	-	-	-	-	+0.9	-	-0.9	-	-1.4	-2.0	-	-
3	14.01 Dec, 1985	6413.51	-57.45	UM2	22.5	30	-	-	-	-	-	-	+0.9	-	-0.8	-	-	-2.2	-	-
4	25.00 Dec, 1985	6424.50	-46.46	UM2	22.5	30	-	+6.7	-	+7.0	+5.2	+2.8	-0.5	-	-1.6	-	-1.6	-3.3	-	-
5	30.00 Dec, 1985	6429.50	-41.46	UM2	22.5	30	-	-	+7.5	+7.5	+6.2	+3.2	-0.1	-	-0.9	-	-1.3	-3.2	-	-
6	1.01 Jan, 1986	6431.51	-39.45	UM2	22.5	30	-	-	-	-	-	-	-	-	-1.5	-	-1.0	-	-	-
7	7.89 Jan, 1986	6438.39	-32.57	UM2	22.5	30	-	-	+5.9	+6.1	+4.1	+1.5	-1.6	-	-2.8	-	-2.8	-4.4	-	-
8	11.1 Jan, 1986	6441.60	-29.36	WIRO	5	16	-	-	-	+7.6	+5.1	+3.6	+0.8	-0.3	-1.0	-0.1	-0.8	-	-2.4	-
9	11.9 Jan, 1986	6442.40	-28.56	WIRO	5	17	-	-	-	+7.56	+5.02	+2.80	-0.72	-1.16	-1.24	-1.61	-1.46	-	-2.41	-2.4
10	12.0 Jan, 1986	6442.50	-28.46	UM2	22.5	30	-	+5.7	+6.3	+6.1	+3.6	+1.3	-2.1	-	-3.1	-	-3.2	-3.3	-	-
11	12.7 Jan, 1986	6443.20	-27.76	WIRO	5	18	-	-	-	+6.69	+4.02	+2.04	-1.11	-1.58	-1.92	-2.19	-2.15	-	-3.17	-3.4
12	12.7 Jan, 1986	6443.20	-27.76	WIRO	5	18	-	-	-	+6.92	+4.34	+2.17	-1.01	-1.40	-1.90	-2.10	-2.10	-	-3.10	-3.4
13	12.8 Jan, 1986	6443.30	-27.66	WIRO	2.2	18	-	-	-	+7.67	+5.35	+3.40	+0.16	-	-0.73	-0.97	-1.05	-	-1.86	-
14	12.8 Jan, 1986	6443.30	-27.66	WIRO	3.3	18	-	-	-	+7.05	+5.43	+3.18	+0.18	-	-1.14	-1.45	-1.29	-	-2.08	-
15	12.9 Jan, 1986	6443.40	-27.56	WIRO	8.3	18	-	-	-	+6.39	+3.56	+1.54	-1.20	-	-2.24	-2.58	-2.33	-	-3.48	-
16	26.8 Jan, 1986	6457.30	-13.60	UM2	22.5	30	-	+4.5	+4.4	+4.5	+1.2	-0.8	-3.6	-	-4.2	-	-4.3	-5.4	-	-
17	9.75 Feb, 1986	6471.25	+00.29	UM2	22.5	30	-	-	-	+3.7	+2.0	-0.3	-2.8	-	-3.9	-	-3.9	-5.1	-	-
18	9.83 Feb, 1986	6471.33	+00.37	WIRO	8.3	18	-	-	-	+4.33	+1.58	-0.28	-2.54	-3.01	-3.84	-3.71	-3.46	-	-	-4.5
19	9.85 Feb, 1986	6471.35	+00.39	UM2	22.5	30	-	-	-	+3.5	+1.8	-1.0	-3.3	-	-4.3	-	-4.2	-5.7	-	-
20	10.72 Feb, 1986	6472.22	+01.26	UM2	22.5	30	-	-	+3.0	+2.6	+0.2	-1.7	-3.8	-	-5.1	-	-4.9	-6.3	-	-
21	10.77 Feb, 1986	6472.27	+01.31	UM2	22.5	30	+4.3	+3.3	+3.0	+2.3	+0.2	-2.1	-4.2	-	-5.5	-	-5.2	-6.6	-	-
22	11.88 Feb, 1986	6473.38	+02.42	WIRO	8.3	20	-	-	-	+3.80	+1.25	-0.54	-2.73	-3.20	-3.94	-3.63	-3.64	-	-4.56	-4.7
23	12.67 Feb, 1986	6474.17	+03.21	UM2	22.5	30	+4.6	+3.7	+3.5	+2.3	-0.2	-1.8	-4.1	-	-5.2	-	-5.1	-6.5	-	-
24.	12.74 Feb, 1986	6474.24	+03.28	UM2	22.5	30	+4.2	+4.2	+3.0	+2.3	-0.1	-1.8	-4.2	-	-5.5	-	-5.3	-6.5	-	-
25	14.67 Feb, 1986	6476.17	+5.21	UM2	22.5	30	-	+4.3	+4.5	+3.1	+1.1	-0.9	-3.8	-	-4.7	-	-4.8	-6.3	-	-
26	14.79 Feb, 1986	6476.29	+05.33	UM2	22.5	30	-	-	-	-	+0.7	-1.3	-3.9	-	-4.8	-	-4.8	-6.0	-	-
27	21.7 Feb, 1986	6483.20	+12.24	UM2	22.5	30	-	-	+5.2	+4.5	+2.1	+0.0	-2.8	-	-3.8	-	-3.9	-5.2	-	-
28	27.69 Feb, 1986	6489.19	+18.23	UM2	22.5	30	+4.9	+4.7	+4.5	+4.1	+1.8	-0.4	-3.5	-	-4.5	-	-4.3	-5.5	-	-
29	27.70 Feb, 1986	6489.20	+18.24	WIRO	8.3	17.5	-	-	-	+4.95	+2.10	+0.24	-2.43	-3.10	-3.52	-3.56	-3.46	-	-3.91	-3.3
30	27.75 Feb, 1986	6489.25	+18.29	UM2	22.5	30	-	-	+4.3	+3.7	+1.3	-0.7	-3.3	-	-4.2	-	-4.0	-5.8	-	-
31	2.71 Mar, 1986	6492.21	+21.25	WIRO	5	5	-	-	-	-	-	-	-	-1.87	-	-	-	-	-	-
32	2.71 Mar, 1986	6492.21	+21.25	WIRO	5	43	-	-	-	+5.84	+3.07	+1.00	-1.71	-2.24	-2.47	-2.94	-2.77	-	-3.57	-3.2
33	4.64 Mar, 1986	6494.14	+23.18	UM2	22.5	30	-	-	-	+5.7	+3.9	+1.4	-1.7	-	-2.5	-	-2.3	-3.2	-	-
34	6.74 Mar, 1986	6496.24	+25.28	WIRO	5	40	-	-	-	+7.65	+4.08	+1.73	-1.40	-1.87	-	-2.64	-2.09	-	-	-
35	7.61 Mar, 1986	6497.11	+26.15	UM2	22.5	30	-	-	+4.2	+4.1	+1.9	-0.4	-3.5	-	-4.2	-	-4.3	-5.6	-	-
36	13.62 Mar, 1986	6503.12	+32.16	WIRO	5	5	-	-	-	-	+5.70	-	-	-0.80	-1.14	-	-	-	-	-
37	13.62 Mar, 1986	6503.12	+32.16	WIRO	5	20	-	-	-	+7.46	+5.23	+2.68	-0.53	-1.27	-1.45	-1.71	-1.58	-	-2.83	-2.8
38	15.63 Mar, 1986	6505.13	+34.17	UM2	22.5	30	-	-	+5.5	+6.0	+3.8	+1.5	-2.2	-	-3.3	-	-3.3	-3.7	-	-
39	20.58 Mar, 1986	6510.08	+39.12	UM2	22.5	30	-	+6.2	-	-	+4.2	+1.8	-1.2	-	-2.5	-	-2.6	-3.8	-	-
40	23.5 Mar, 1986	6513.00	+42.04	UM2	22.5	30	-	-	-	+6.4	+5.0	+2.3	-1.6	-	-2.5	-	-3.2	-	-	-
41	25.5 Mar, 1986	6515.00	+44.04	MLOF	15.2	23	-	+7.49	+7.27	+7.31	+4.93	+2.76	-1.27	-2.03	-1.92	-2.32	-2.70	-3.2:	-	-
42	28.55 Mar, 1986	6518.05	+47.09	WIRO	5	17	-	-	-	+7.94	+6.14	+3.42	+0.03	-0.83	-1.15	-1.49	-1.60	-	-2.65	-2.58
43	27.3 Apr, 1986	6547.80	+76.84	MLOF	10	20	-	-	-	≥+8.1	-	-	+0.8	-	-0.2	-	-0.6	-	-	-
44	28.3 Apr, 1986	6548.80	+77.84	MLOF	10	20	-	-	+9.2	-	-	≥+6.0	+1.1	-	-0.1	-	-0.7	-1.5	-	-
45	1.21 May, 1986	6551.71	+80.75	WIRO	5	20	-	-	-	+9.81	+8.44	+5.67	+2.44	+1.15	+0.85	+0.39	-0.21	-	-0.96	-0.81
46	5.2 May, 1986	6555.70	+84.74	UM2	22.5	30	-	-	-	-	-	-	+0.4	-	-0.7	-	-1.2	-	-	-
47	6.2 May, 1986	6556.70	+85.74	UM2	22.5	30	-	-	≥+7.6	-	≥+6.0	≥+3.7	+1.0	-	-0.0	-	-0.9	-	-	-
COMET KOBAYASHI-BERGER-MILON 1975 IX																				
1	27. Jul, 1975	2621.2	-39.6	UM1	30.3	30	-	-	-	-	-	-	+1.1	-	0.0	-	-0.7	-	-	-
2	27.7 Aug, 1975	2652.2	-08.6	UM1	30.3	30	-	+5.1	+5.3	+5.6	+2.6	+0.5	-2.1	-	-2.8	-	-3.1	-	-	-
3	31.9 Aug, 1975	2656.4	-04.4	UM1	30.3	30	-	+5.6	+5.7	+5.3	+2.0	+0.2	-2.3	-	-3.0	-	-3.1	-	-	-
4	1.9 Sep, 1975	2657.4	-03.4	UM1	30.3	30	-	+5.3	+5.1	+5.0	+2.1	+0.5	-2.1	-	-2.8	-	-3.1	-	-	-

TABLE II—*Continued*

(1)	(2)	(3)	(4)	(5)	(6)	(7)	(8)	(9)	(10)	(11)	(12)	(13)	(14)	(15)	(16)	(17)	(18)	(19)	(20)	(21)
#	UT DATE	JD 2,440,000+	Days from Perihelion	SYSTEM	ϕ arcsec	ψ arcsec	[0.7]	[1.2]	[1.6]	[2.X][2]	[3.6]	[4.X][2]	[8.X][2]	N	[10.X][2]	[11.X][2]	[12.X][2]	[18]	[19.5]	[23]
5	2.7 Sep, 1975	2658.2	-02.6	UM1	30.3	30	-	+5.2	+5.0	+5.2	+2.0	+0.3	-2.2	-	-2.9	-	-3.2	-	-	-
6	3.9 Sep, 1975	2659.4	-01.4	UM1	30.3	30	-	+5.6	+5.7	+5.0	+1.8	-0.4	-2.6	-	-3.0	-	-3.5	-	-	-
7	5.3 Sep, 1975	2660.8	-00.0	UM1	30.3	30	-	-	-	+5.4	+2.0	+0.4	-2.1	-	-2.9	-	-3.2	-	-	-
8	8.8 Sep, 1975	2664.3	+3.5	UM1	30.3	30	-	+6.5	+6.3	+6.0	+2.0	+0.5	-2.2	-	-2.9	-	-3.1	-	-	-
COMET BRADFIELD 1980 XV (1980t)																				
1	1.8 Jan, 1981	4606.3	+03.3	UM2	22.5	30	-	+2.2	+1.8	+1.4	-0.6	-1.9	-3.6	-	-4.6	-	-4.6	-4.6	-	-
2	2.8 Jan, 1981	4607.3	+04.3	UM2	22.5	30	+4.1	+3.0	+2.7	+1.7	-0.5	-1.9	-3.7	-	-4.5	-	-4.5	-4.9	-	-
3	3.8 Jan, 1981	4608.3	+05.3	UM2	22.5	30	+4.9	+3.8	+3.3	+2.6	0.0	-1.6	-3.7	-	-4.4	-	-4.4	-5.0	-	-
4	9.7 Jan, 1981	4614.2	+11.2	UM2	22.5	30	+7.8	+6.4	+6.2	+5.7	+2.7	+0.6	-2.2	-	-2.9	-	-2.9	-3.4	-	-
5	11.9 Jan, 1981	4616.4	+13.4	UM2	22.5	30	+8.2	+7:	+7:	+6.3	+3.5	+1.2	-1.7	-	-2.3	-	-2.4	-3.2	-	-
6	16.8 Jan, 1981	4621.3	+18.3	UM2	22.5	30	-	+6.2	+6.3	+6.2	+3.5	+1.1	-2:	-	-2.7	-	-2.9	-3.7	-	-
7	17.9 Jan, 1981	4622.4	+19.4	UM2	22.5	30	+8.5	+7.2	-	+6.5	+4:	+1.9	-1.5	-	-2.2	-	-2.4	-2.7	-	-
8	18.8 Jan, 1981	4623.3	+20.3	UM2	22.5	30	-	+6.8	+7.5	+6.8	+4.3	+2:	-1.2	-	-1.9	-	-2.1	-3.2	-	-
9	21.8 Jan, 1981	4626.3	+23.3	UM2	22.5	30	-	-	-	+7.6	+5.4	+3.2	-0.6	-	-1.2	-	-1.5	-2.5	-	-
10	22.9 Jan, 1981	4627.4	+24.4	WIRO	8.3	20	-	-	-	-	+6.53	+4.21	+1.02	+0.66	-	+0.18	-0.05	-	-1.27	-
11	22.9 Jan, 1981	4627.4	+24.4	WIRO	5	20	-	-	-	-	+7.01	+4.66	+1.56	+1.09	-	+0.55	+0.20	-	-0.49	-
12	24.8 Jan, 1981	4629.3	+26.3	UM2	22.5	30	-	-	-	-	+6.0	+3.1	+0.4	-	-0.7	-	-0.8	-	-	-
COMET AUSTIN 1984 XIII (1984i)																				
1	8.8 Aug, 1984	5921.3	-03.3	UM2	22.5	30	-	-	-	-	-	-0.66	-3.05	-	-3.63	-	-3.77	-	-	-
2	9.8 Aug, 1984	5922.3	-02.3	UM2	22.5	30	-	+5.00	+4.84	+3.55	+0.65	-1.07	-2.98	-	-3.42	-	-3.66	-	-	
3	10.8 Aug, 1984	5923.3	-01.3	UM2	22.5	30	-	+4.8	+4.5	+3.51	+0.42	-1.16	-3.16	-	-3.62	-	-3.89	-	-	-
COMET MACHHOLZ 1985 VIII (1985e)																				
1	24.75 Jan, 1985	6241.25		UM2	22.5	30	-	+4.2	≥+5.6	+4.4	+1.5	-0.1	-1.3	-	-1.9	-	-2.0	-	-	-
COMET AUSTIN (1989c$_1$)																				
1	23.83 Mar, 1990	7974.33	-17.14	UM2	22.5	30	-	-	-	-	-	-	-1.0	-	-	-	-	-	-	-
2	3.71 Apr, 1990	7985.21	-6.26	UM2	22.5	30	-	-	+5.6	+5.2	+2.1	-0.1	-2.3	-	-2.9	-	-3.1	-3.5	-	-
3	12.78 Apr, 1990	7994.28	+2.81	UM2	22.5	30	-	-	-	+5.3	+1.5	-0.3	-2.7	-	-3.5	-	-3.7	-	-	-
4	15.79 Apr, 1990	7997.29	+5.82	WIRO	5	50	-	+6.91	-	+5.88	+2.89	+1.04	-0.65	-1.12	-1.48	-1.38	-1.84	-2.06	-	-
COMET BRORSON-METCALF X (1989o)																				
1	15.8 Sep, 1989	7785.3	+3.86	WIRO	5	27	-	-	-	≥+7.6	+5.58	+4.16	+1.27	+0.87	+0.90	+0.89	+0.92	-0.62	-	-
2	16.7 Sep, 1989	7786.2	+4.76	WIRO	5	24	-	≥+8.1	≥+8.7	-	+6.36	+3.92	+1.69	+1.07	+1.15	+0.60	+0.59	+0.30	-	-
PRIMARY CALIBRATOR																				
VEGA				WIRO	5	-	0.00	-0.01	-0.01	-0.02	-0.03	-0.03	-0.03	-0.03	-0.03	-0.03	-0.03	-0.03	-0.03	-0.03
VEGA				UM1,2	22.5	-	0.0	0.0	0.0	0.0	0.0	0.0	0.0	0.0	0.0	0.0	0.0	0.0	0.0	0.0

[1]UM1 had a 27" square beam which is equivalent to a 30.3" circular aperture; UM2 had a 20" square beam which is equivalent to a 22.5" circular aperture; MLOF on 25 March, 1986 UT had a 13.5" square beam which is equivalent to a 15.2" circular aperture.
[2]Effective wavelengths for the UM system are 2.2, 4.8, 8.5, 10.6, and 12.5μm; effective wavelengths for the WIRO system are 2.3, 4.9, 8.7, 10, 11.4 and 12.6μm; effective wavelengths for the MLOF system are 2.3, 4.9, 8.6, 10.3, 11.3, and 12.8μm.

Many of the arguments in the analysis below are based upon the assumption that the infrared energy distributions measure the properties of the optically important grains. It is known from dust impact measurements with the *Giotto* spacecraft that there was a large range of particle sizes in the coma of P/Halley, and that the differential particle mass distribution followed a power law (see McDonnell *et al.* 1987). A power law grain-size distribution has also been found to be consistent with the thermal emission from other comets (see Hanner *et al.* 1985a, 1985c). Jewitt and Meech (1986) and Jewitt (1991) have argued that the effective grain radius a for the grains that are optically important can be determined by computing the optically weighted mean grain size, assuming that the differential grain distribution follows a power law of the form $n(a)da = Ka^{-m}da$, where m lies between 3 and 4.5. If one

TABLE III
Measured Properties of Comet P/Halley and Six Other Recent Bright Comets

(1)	(2)	(3)	(4)	(5)	(6)	(7)	(8)	(9)	(10)	(11)	(12)	(13)	(14)	(15)	(16)	(17)	(18)
#	UT Date	JD 2,440,000+	Days from Perihelion	SYSTEM	r AU	Δ AU	T_{BB} K	T_{color} K	S	$[\lambda f_\lambda(IR)]_{max}$	$[\lambda f_\lambda(V)]_{max}$	A(θ)	θ, mas	a km	$\frac{1}{r^4\Delta}$	$\left[\frac{4\psi}{4\psi-\phi}\right]\left[\frac{20}{\phi}\right]$	$[\lambda f_\lambda(IR)]_{max} \times r^4\Delta\left[\frac{4\psi}{4\psi-\phi}\right]\left[\frac{20}{\phi}\right]$
COMET P/HALLEY 1986 III																	
1	12.11 Dec, 1985	6411.61	-59.35	UM	1.32	0.77	242	331	1.37	3.5×10^{-15}	8.4×10^{-16}	0.19	54	30.5	0.43	1.09	8.88×10^{-15}
2	13.06 Dec, 1985	6412.56	-58.40	UM	1.30	0.79	244	306	1.25	1.0×10^{-15}	-	-	34	19.6	0.44	1.09	2.47×10^{-15}
3	14.01 Dec, 1985	6413.51	-57.45	UM	1.29	0.80	245	-	-	1×10^{-15}	-	-	-	-	0.45	1.09	2.42×10^{-15}
4	25.00 Dec, 1985	6424.50	-46.46	UM	1.12	1.02	263	382	1.45	2.9×10^{-15}	1.1×10^{-15}	0.28	37	27.6	0.62	1.09	5.09×10^{-15}
5	30.00 Dec, 1985	6429.50	-41.46	UM	1.04	1.12	273	328	1.20	2.6×10^{-15}	6.5×10^{-16}	0.20	48	39.0	0.76	1.09	3.73×10^{-15}
6	1.01 Jan, 1986	6431.51	-39.45	UM	1.01	1.16	277	-	-	1.8×10^{-15}	-	-	-	-	0.83	1.09	2.36×10^{-15}
7	7.89 Jan, 1986	6438.39	-32.57	UM	0.90	1.29	293	382	1.30	9×10^{-15}	2.1×10^{-15}	0.19	66	61.6	1.18	1.09	8.31×10^{-15}
8	11.1 Jan, 1986	6441.60	-29.36	WIRO	0.86	1.34	300	-	-	-	-	-	-	-	1.36	4.32	
9	11.9 Jan, 1986	6442.40	-28.56	WIRO	0.85	1.35	302	370	1.21	3×10^{-15}	-	-	40	39.4	1.42	4.32	9.13×10^{-15}
10	12.0 Jan, 1986	6442.50	-28.46	UM	0.85	1.36	302	399	1.32	1×10^{-14}	2.2×10^{-15}	0.18	63	62.7	1.48	1.09	7.37×10^{-15}
11	12.7 Jan, 1986	6443.20	-27.76	WIRO	0.84	1.36	304	375	1.22	5×10^{-15}	-	-	51	50.2	1.48	4.28	1.45×10^{-14}
12	12.7 Jan, 1986	6443.20	-27.76	WIRO	0.84	1.36	304	375	1.22	5×10^{-15}	-	-	51	50.2	1.48	4.28	1.45×10^{-14}
13	12.8 Jan, 1986	6443.30	-27.66	WIRO	0.84	1.36	304	375	1.22	2×10^{-15}	-	-	32	31.8	1.48	9.36	1.26×10^{-14}
14	12.8 Jan, 1986	6443.30	-27.66	WIRO	0.84	1.36	304	375	1.22	2×10^{-15}	-	-	32	31.8	1.48	6.36	8.59×10^{-15}
15	12.9 Jan, 1986	6443.40	-27.56	WIRO	0.84	1.36	304	375	1.22	6×10^{-15}	-	-	56	55	1.48	2.72	1.10×10^{-14}
16	26.8 Jan, 1986	6457.30	-13.60	UM	0.66	1.54	343	427	1.24	5×10^{-14}	1×10^{-14}	0.17	124	139	3.42	1.04	1.52×10^{-14}
17	9.75 Feb, 1986	6471.25	+00.29	UM	0.59	1.54	362	459	1.27	2.9×10^{-14}	-	-	82	91	5.36	1.04	5.63×10^{-15}
18	9.83 Feb, 1986	6471.33	+00.37	WIRO	0.59	1.54	362	470	1.28	2×10^{-14}	-	-	65	73	5.36	2.72	1.01×10^{-14}
19	9.85 Feb, 1986	6471.35	+00.39	UM	0.59	1.54	362	439	1.21	3.8×10^{-14}	-	-	102	114	5.36	1.09	7.73×10^{-15}
20	10.72 Feb, 1986	6472.22	+01.26	UM	0.59	1.54	362	517	1.43	8×10^{-14}	-	-	106	120	5.36	1.09	1.64×10^{-14}
21	10.77 Feb, 1986	6472.27	+01.31	UM	0.59	1.54	362	496	1.37	1.05×10^{-13}	2.8×10^{-14}	0.21	133	150	5.36	1.09	2.14×10^{-14}
22	11.88 Feb, 1986	6473.38	+02.42	WIRO	0.59	1.53	362	470	1.28	2.5×10^{-14}	-	-	72	80	5.39	2.70	1.25×10^{-14}
23	12.67 Feb, 1986	6474.17	+03.21	UM	0.59	1.52	362	496	1.37	9.1×10^{-14}	2.36×10^{-14}	0.21	124	137	5.43	1.09	1.82×10^{-14}
24	12.74 Feb, 1986	6474.24	+03.28	UM	0.59	1.52	362	459	1.27	1.09×10^{-13}	2.58×10^{-14}	0.19	158	175	5.43	1.09	2.19×10^{-14}
25	14.67 Feb, 1986	6476.17	+5.21	UM	0.60	1.50	359	402	1.12	6.51×10^{-14}	1.07×10^{-14}	0.14	159	174	5.14	1.09	1.38×10^{-14}
26	14.79 Feb, 1986	6476.29	+05.33	UM	0.60	1.50	359	427	1.19	7.3×10^{-14}	-	-	150	163	5.14	1.09	1.55×10^{-14}
27	21.7 Feb, 1986	6483.20	+12.24	UM	0.65	1.40	345	405	1.17	2.64×10^{-14}	4.44×10^{-15}	0.15	100	102	4.00	1.09	7.19×10^{-15}
28	27.69 Feb, 1986	6489.19	+18.23	UM	0.71	1.29	330	395	1.20	4.44×10^{-14}	1.2×10^{-14}	0.21	136	128	3.05	1.09	1.59×10^{-14}
29	27.70 Feb, 1986	6489.20	+18.24	WIRO	0.71	1.29	330	432	1.30	1.5×10^{-14}	-	-	66	62	3.05	2.72	1.34×10^{-14}
30	27.75 Feb, 1986	6489.25	+18.29	UM	0.71	1.29	330	448	1.36	3.7×10^{-14}	1×10^{-14}	0.21	97	91	3.05	1.09	1.32×10^{-14}
31	2.71 Mar, 1986	6492.21	+21.25	WIRO	0.75	1.22	321	-	-	-	-	-	-	-	2.59	5.32	-
32	2.71 Mar, 1986	6492.21	+21.25	WIRO	0.75	1.22	321	422	1.30	9×10^{-15}	-	-	54	48	2.59	4.12	1.85×10^{-14}
33	4.64 Mar, 1986	6494.14	+23.18	UM	0.76	1.20	319	395	1.24	7.94×10^{-15}	-	-	58	50	2.50	1.09	3.46×10^{-15}
34	6.74 Mar, 1986	6496.24	+25.28	WIRO	0.80	1.13	311	367	1.17	6.5×10^{-15}	-	-	60	50	2.16	4.12	1.24×10^{-14}
35	7.61 Mar, 1986	6497.11	+26.15	UM	0.81	1.12	309	377	1.22	4.64×10^{-14}	1.05×10^{-14}	0.19	153	125	2.13	1.09	2.37×10^{-14}
36	13.62 Mar, 1986	6503.12	+32.16	WIRO	0.90	0.97	293	334	1.13	3.3×10^{-15}	-	-	52	37	1.57	5.32	1.12×10^{-14}
37	13.62 Mar, 1986	6503.12	+32.16	WIRO	0.90	0.97	293	367	1.25	3.5×10^{-15}	-	-	44	31	1.57	4.28	9.53×10^{-15}
38	15.63 Mar, 1986	6505.13	+34.17	UM	0.92	0.92	290	363	1.25	1.2×10^{-14}	2.7×10^{-15}	0.19	84	56	1.50	1.09	8.72×10^{-15}
39	20.58 Mar, 1986	6510.08	+39.12	UM	1.00	0.80	278	375	1.35	6.5×10^{-15}	2.01×10^{-15}	0.24	58	34	1.25	1.09	5.66×10^{-15}
40	23.5 Mar, 1986	6513.00	+42.04	UM	1.05	0.72	272	338	1.24	1.0×10^{-14}	-	-	88	46	1.14	1.09	9.57×10^{-15}
41	25.5 Mar, 1986	6515.00	+44.04	MLOF	1.08	0.68	268	322	1.19	7×10^{-15}	6.0×10^{-16}	0.08	81	40	1.08	1.58	1.06×10^{-14}
42	28.55 Mar, 1986	6518.05	+47.09	WIRO	1.13	0.60	262	322	1.22	2.5×10^{-15}	-	-	47	21	1.04	4.32	1.04×10^{-14}
43	27.3 Apr, 1986	6547.80	+76.84	MLOF	1.57	0.69	222	-	-	1.3×10^{-15}	-	-	-	-	0.24	2.28	1.24×10^{-14}
44	28.3 Apr, 1986	6548.80	+77.84	MLOF	1.59	0.72	220	-	1.46	1.1×10^{-15}	-	-	35	17.6	0.22	2.28	1.35×10^{-14}
45	1.21 May, 1986	6551.71	+80.75	WIRO	1.63	0.80	218	291	1.32	7×10^{-16}	-	-	32	18.4	0.18	4.28	1.66×10^{-14}
46	5.2 May, 1986	6555.70	+84.74	UM	1.69	0.92	214	-	-	1.7×10^{-15}	-	-	-	-	0.13	1.09	1.44×10^{-14}
47	6.2 May, 1986	6556.70	+85.74	UM	1.71	0.96	213	280	1.31	1.06×10^{-15}	-	-	42	29	0.12	1.09	9.63×10^{-15}

TABLE III—*Continued*

(1) #	(2) UT Date	(3) JD 2,440,000+	(4) Days from Perihelion	(5) SYSTEM	(6) r AU	(7) Δ AU	(8) T_{BB} K	(9) T_{color} K	(10) S	(11) $[\lambda f_\lambda(IR)]_{max}$	(12) $[\lambda f_\lambda(V)]_{max}$	(13) A(θ)	(14) θ_r mas	(15) a km	(16) $\frac{1}{r^4\Delta}$	(17) $\left[\frac{4\Psi}{4\Psi-\Phi}\right]\left[\frac{20}{\Phi}\right]$	(18) $[\lambda f_\lambda(IR)]_{max} \times r^4\Delta\left[\frac{4\Psi}{4\Psi-\Phi}\right]\left[\frac{20}{\Phi}\right]$
COMET KOBAYASHI-BERGER-MILON 1975 IX																	
1	27.7 Jul, 1975	2621.2	-39.6	UM1	1.02	0.32	275	-	-	$\sim 1.1\times10^{-15}$	-	-	-	-	2.89	0.88	3.35×10^{-16}
2	27.7 Aug, 1975	2652.2	-08.6	UM1	0.48	0.99	401	427	1.06	1.4×10^{-14}	5.5×10^{-15}	0.28	66	48	19.0	0.88	6.48×10^{-16}
3	31.9 Aug, 1975	2656.4'	-04.4	UM1	0.44	1.09	419	459	1.10	1.7×10^{-14}	3.2×10^{-15}	0.16	62	50	24.5	0.88	6.11×10^{-16}
4	1.9 Sep, 1975	2657.4	-03.4	UM1	0.44	1.11	419	432	1.03	1.5×10^{-14}	5.2×10^{-15}	0.26	66	53	24.0	0.88	5.50×10^{-16}
5	2.7 Sep, 1975	2658.2	-02.6	UM1	0.43	1.12	424	432	1.02	1.5×10^{-14}	5.5×10^{-15}	0.27	66	54	26.1	0.88	6.02×10^{-16}
6	3.9 Sep, 1975	2659.4	-01.4	UM1	0.43	1.15	424	459	1.08	2.4×10^{-14}	3.2×10^{-15}	0.12	74	62	25.4	0.88	8.32×10^{-16}
7	5.3 Sep, 1975	2660.8	-0.0	UM1	0.43	1.17	424	432	1.02	1.7×10^{-14}	-	-	71	61	25.0	0.88	5.98×10^{-16}
8	8.8 Sep, 1975	2664.3	+3.5	UM1	0.44	1.24	419	432	1.03	1.5×10^{-14}	1.7×10^{-15}	0.10	66	60	21.5	0.88	6.14×10^{-16}
COMET BRADFIELD 1980 XV (1980t)																	
1	1.8 Jan, 1981	4606.3	+03.3	UM2	0.28	0.73	525	592	1.13	7×10^{-14}	10^{-13}	0.59	76	40	222.9	1.09	3.43×10^{-16}
2	2.8 Jan, 1981	4607.3	+4.3	UM2	0.30	0.75	508	573	1.13	7×10^{-14}	3.6×10^{-14}	0.34	81	44	164.6	1.09	4.63×10^{-16}
3	3.8 Jan, 1981	4608.3	+5.3	UM2	0.31	0.77	499	510	1.02	6.5×10^{-14}	1.5×10^{-14}	0.19	99	55	140.6	1.09	5.04×10^{-16}
4	9.7 Jan, 1981	4614.2	+11.2	UM2	0.44	0.96	419	432	1.03	1.2×10^{-14}	1.6×10^{-15}	0.12	59	41	27.8	1.09	4.71×10^{-16}
5	11.9 Jan, 1981	4616.4	+13.4	UM2	0.49	1.04	397	427	1.08	8×10^{-15}	8×10^{-16}	0.09	50	44	16.7	1.09	5.22×10^{-16}
6	16.8 Jan, 1981	4621.3	+18.3	UM2	0.61	1.23	356	386	1.08	1.2×10^{-14}	1.9×10^{-15}	0.14	74	66	5.9	1.09	2.22×10^{-15}
7	17.9 Jan, 1981	4622.4	+19.4	UM2	0.64	1.27	348	367	1.05	5.5×10^{-15}	6×10^{-16}	0.10	56	51	4.7	1.09	1.28×10^{-15}
8	18.8 Jan, 1981	4623.3	+20.3	UM2	0.66	1.30	342	386	1.13	5×10^{-15}	8×10^{-16}	0.14	48	45	4.1	1.09	1.33×10^{-15}
9	21.8 Jan, 1981	4626.3	+23.3	UM2	0.72	1.41	328	367	1.12	3.2×10^{-15}	-	-	42	44	2.6	1.09	1.34×10^{-15}
10	22.9 Jan, 1981	4627.4	+24.4	WIRO	0.75	1.44	321	376	1.17	6.5×10^{-16}	-	-	18	19	2.2	2.72	10^{-16}
11	22.9 Jan, 1981	4627.4	+24.4	WIRO	0.75	1.44	321	367	1.14	5×10^{-16}	-	-	17	17.6	2.2	4.28	10^{-16}
12	24.8 Jan, 1981	4629.3	+26.3	UM2	0.79	1.51	313	380	1.21	1.6×10^{-15}	-	-	28	37	1.7	1.09	1.03×10^{-15}
COMET AUSTIN 1984 XIII (1984i)																	
1	8.8 Aug, 1984	5921.3	-03.3	UM2	0.31	1.16	499	-	-	3×10^{-14}	-	-	79	67	93.3	1.09	3.50×10^{-16}
2	9.8 Aug, 1984	5922.3	-02.3	UM2	0.30	1.19	508	540	1.06	3.4×10^{-14}	6.8×10^{-15}	0.17	64	55	103.7	1.09	3.57×10^{-16}
3	10.8 Aug, 1984	5923.3	-01.3	UM2	0.30	1.22	508	524	1.03	4×10^{-14}	8×10^{-15}	0.17	74	65	101.2	1.09	4.31×10^{-16}
COMET MACHHOLZ 1985 VIII (1985e)																	
1	24.75 Jun, 1985	6241.25	-4.0	UM2	0.22	1.09	593	667	1.12	10^{-14}	-	-	23	18	391.6	1.09	2.79×10^{-17}
COMET AUSTIN (1989c$_1$)																	
1	23.83 Mar, 1990	7974.33	-17.14	UM2	0.59	1.36	362	-	-	5×10^{-15}	-	-	-	-	6.07	1.09	8.98×10^{-16}
2	3.71 Apr, 1990	7985.21	-6.26	UM2	0.39	1.16	445	459	1.03	1.6×10^{-14}	3.4×10^{-15}	0.17	61	51	37.3	1.09	4.67×10^{-16}
3	12.78 Apr, 1990	7994.28	+2.81	UM2	0.36	0.96	463	458	0.99	2.4×10^{-14}	-	-	75	52	62.0	1.09	4.22×10^{-16}
4	15.79 Apr, 1990	7997.29	+5.82	WIRO	0.39	0.88	445	524	1.18	4.5×10^{-15}	1.2×10^{-15}	0.21	25	15.8	49.1	4.12	3.78×10^{-16}
COMET BRORSON-METCALF 1989 X (1989o)																	
1	15.8 Sep, 1989	7785.3	+3.86	WIRO	0.49	1.23	398	408	1.03	6×10^{-16}	-	-	15	13.3	14.10	4.22	1.8×10^{-16}
2	16.7 Sep, 1989	7786.2	+4.76	WIRO	0.49	1.25	398	432	1.09	4×10^{-16}	-	-	11	9.8	13.88	4.20	1.21×10^{-16}

assumes that there is a lower limit a_{min} to the grain radius and that the value of m lies close to 4.5 or even 5 (see Hayward *et al.* 1986), then the optically weighted mean grain size is given by $2a_{min} \leq a \leq 3a_{min}$. The effective radius of the optically important grains in comets is nearly an order of magnitude larger than the effective radius of the grains responsible for the general interstellar extinction. Jewitt and Meech (1986) suggest that the grains incorporated in comet nuclei during the formation of the Solar System could have grown to the larger radii characteristic of comet grains by accretion in the cores of molecular clouds. In fact, optical/infrared extinction and polarization studies provide strong evidence that the grains in the Orion nebula (Breger *et al.* 1981) and the Ophiuchus Dark Cloud (Castelaz *et al.* 1985) are larger than interstellar grains. Small grains were detected in the coma of P/Halley by the *Giotto* dust detectors, but the differential size distribution flattens out below grain radii of ≈ 0.5 μm (McDonnell *et al.* 1987, 1991), so that the small grains do not contribute significantly to the optical scattering and emission from the coma (see also Hanner 1988, Jewitt 1991). We assume in the discussion that follows that the grain radius measured by the infrared emission is the optically weighted mean defined above.

We have assumed in our analysis that the grains in the coma are radiatively cooled, and that heat losses by conduction to the gas are negligible. In the steady-state model (see Appendix A), the grains are accelerated to terminal velocity by momentum coupling to the gas. The hydrodynamic coupling is through the viscosity of the plasma. Since the transport properties of viscosity and thermal conductivity are proportional to each other (and to $T^{1/2}$), the grains are thermally coupled to the gas as long as they are being accelerated by the gas. The density of the gas in the outflow decreases inversely as the square of the distance from the nucleus. When the gas mean free path, which is inversely proportional to the gas density, approaches the size of the grains, the coupling to the gas is reduced and both the thermal conductivity and the viscosity become proportional to the pressure. In general, we do not know the coma radius at which this condition occurs, but from this point outward the grains cool radiatively, and the relationship between flux and diaphragm diameter is linear (see Eq. A-4). Visible images of Comet Levy 1990c with the Hubble Space Telescope show that this linear relationship holds to diaphragm radii as small as 0.1 arcsec (Weaver *et al.* 1992). We therefore believe that it is safe to assume that cooling of the grains by thermal conduction to the gas can be ignored for the coma in the observing diaphragms we used in this study (radii of 1.1 to 13.5 arcsec).

A. General Morphology of the Energy Distributions

Figures 1–3 display typical infrared energy distributions exhibited by P/Halley and the six other recent comets measured in this study. We have included the energy distributions of the coma, tail, and anti-tail of Comet Kohoutek (Ney 1974a) in Fig. 1 for comparison. In all cases (except Machholz, which was too faint for our O'Brien detector at short wavelengths) there was a clearly defined visible/near-infrared continuum due to reflected sunlight and a thermal-infrared component due to thermal emission from dust. Both these components have been observed previously in many comets (see Ney 1982a). The comets in our study appear to fall into two basic classes based upon their thermal infrared dust emission (Figs. 2 and 4–6): I, those that show continuum emission with low superheat and weak or muted silicate emission features (designated IR Type I by Gehrz *et al.* 1989), and II, those that have optically thin 10- and 20-μm silicate emission features (Woolf and Ney 1969) superimposed on a superheated thermal infrared continuum believed to be caused by emission from small carbon or iron grains (designated IR Type II by Gehrz *et al.* 1989). The IR Type I/II designation assigned by Gehrz *et al.* (1989) was based upon the fact that the IR Type I comets had Type I (ion) tails, and the IR Type II comets were characterized by the presence

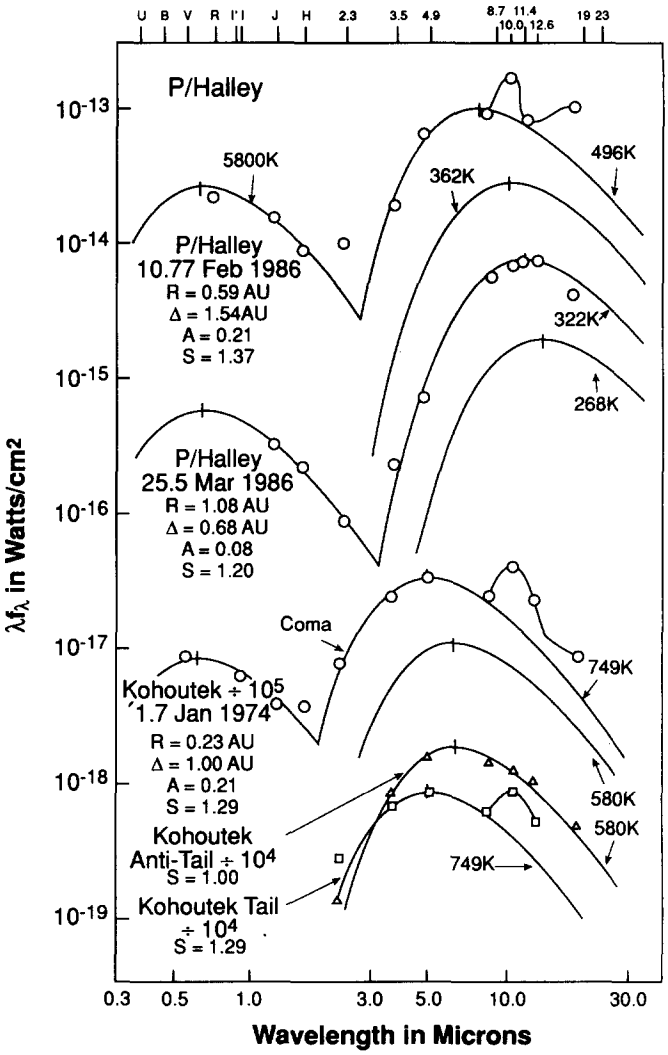

FIG. 1. Typical coma energy distributions for P/Halley when the 10-μm silicate emission feature was present (10.77 February 1986 UT) and absent (25.5 March 1986 UT) showing the scattered solar and thermal continua. Statistical errors are smaller than the plotting symbols. R is the heliocentric distance in AU, Δ is the geocentric distance in AU, A is the albedo, and S is the superheat. The energy distributions of the coma, dust tail, and antitail of Comet Kohoutek are included for comparison (data for Ney 1974a). Also shown are blackbody energy distributions corresponding to the black sphere temperature at the heliocentric distance of each comet as given by Eq. (3).

of prominent Type II (dust) tails. It is evident from Figs. 1 and 3 that there were occasions upon which P/Halley, normally an IR Type II comet, became an IR Type I comet.

The differences between the dust emission from IR Types I and II comets could be caused by effects that are dependent upon grain size. The energy distributions of the IR Type II comets are similar to those of Kohoutek's Type II dust tail and coma which were composed of small

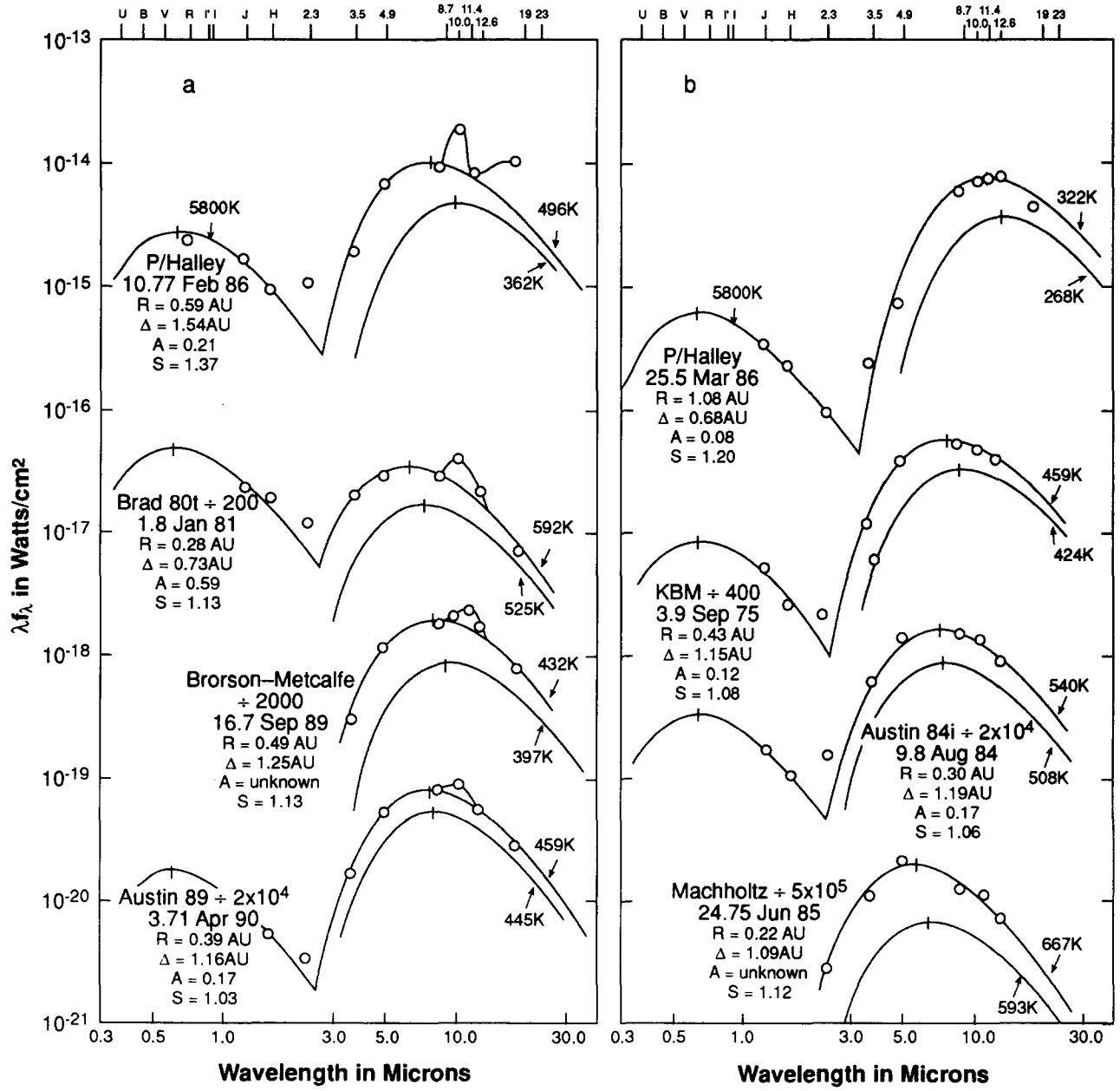

FIG. 2. The energy distributions of six recent bright comets compared to P/Halley. The quantities R, Δ, A, and S are as defined in Fig. 1. Statistical errors are smaller than the plotting symbols. Panel (a) shows comets whose energy distributions are characterized by 10- and 20-μm silicate features superimposed on a smooth continuum caused by thermal emission from carbon or iron grains. Panel (b) shows the IR Type I comets in our survey.

grains (less than 1 μm in diameter) with an optically thin silicate component. IR Type I comets have energy distributions more like that of the anti-tail of Comet Kohoutek. Ney (1974a) has argued that the anti-tail is composed of "gravel" (diameters greater than 1 mm) in the plane of the comet orbit (see also Sekanina 1974a,b, 1976). The coma and dust-tail grains of Kohoutek and the coma grains of the IR Type II comets are superheated as defined in Section B, the anti-tail grains of Kohoutek are not superheated at all, and the superheat of the coma grains of the IR Type I comets is small.

B. Comet Grain Properties

Spectral energy distributions of the comets in our sample (Table II and Figs. 1–7) can be used to determine:

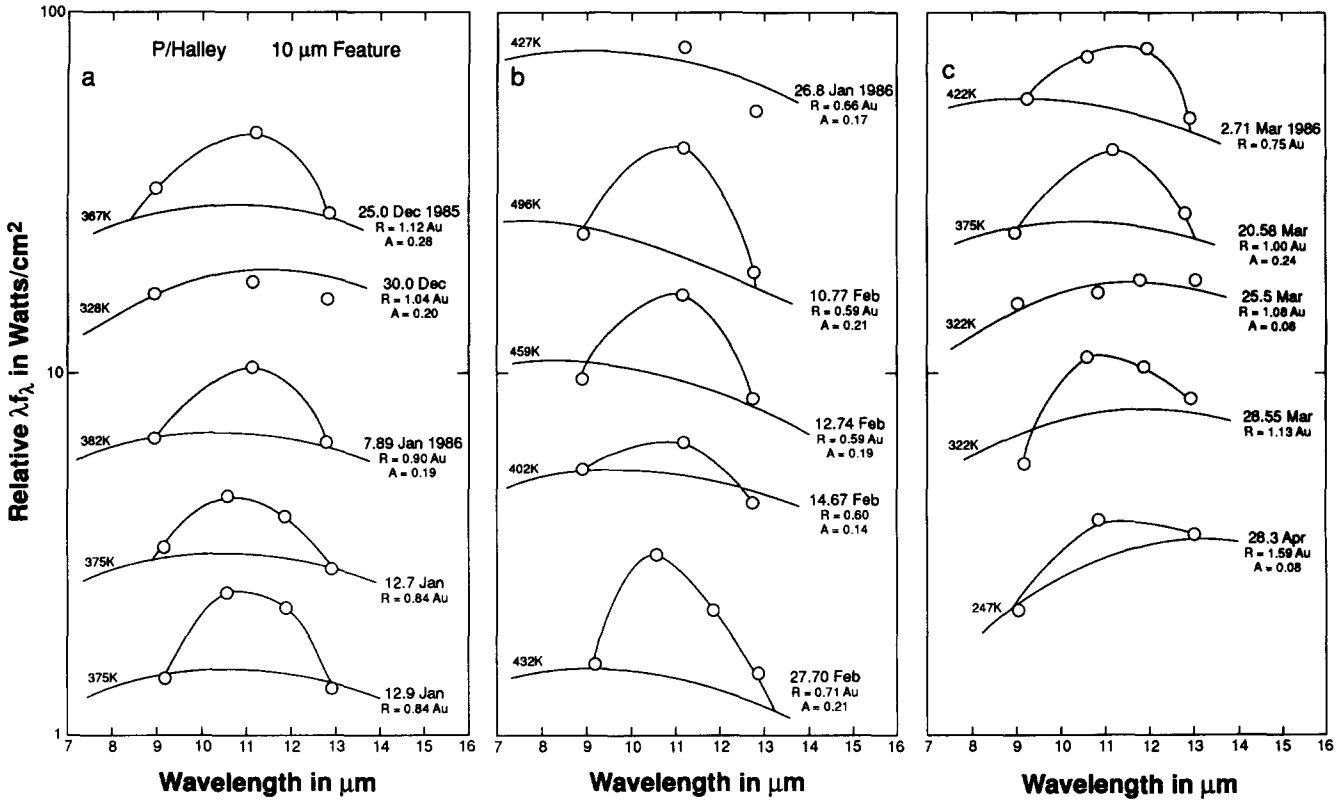

FIG. 3. The 7- to 14-μm energy distribution of P/Halley showing temporal variations observed in the contrast of the 10-μm silicate emission feature. R and S are as defined in Fig. 1. Statistical errors are smaller than the plotting symbols. The silicate feature was occasionally weak or absent for heliocentric distances both less than and larger than 1 AU. On 25.5 March, when the signature was absent, the albedo of P/Halley fell to about 0.08. The blackbody curves were determined from the continuum outside the feature.

1, the mineral content of the grains; 2, the rough size distribution of the grains responsible for the thermal infrared emission; 3, some structural properties of the grains; and 4, the temporal variability of these properties.

The mineral composition of comet grains. The 10- and 20-μm emission features in the IR Type II comets indicate that there is an optically thin silicate dust component in the coma. These features, observed first in a comet (Bennett 1969i) by Maas *et al.* (1970), suggest that IR Type II comets contain the same type of silicate materials observed in the circumstellar shells of cool supergiant stars (Woolf and Ney 1974). Silicate emission features are usually, though not always, present in P/Halley spectra as discussed below (Figs. 1 and 3). Recent determinations of the composition of P/Halley's coma grains by the *Giotto* PIA mass spectrometer appear to confirm the presence of iron–magnesium silicate material in the inner coma (Kissel *et al.* 1986). The thermal continuum radiation from 3 to 8 μm that is present in both IR Type I and IR Type II comets is believed to be due to carbon or iron (Ney 1982a); we assume in the following discussion that the material responsible for this thermal continuum emission is carbon.

P/Halley is the only periodic comet among the seven observed in this study; the remainder are new comets. Although previous studies (Ney 1974a, 1982a) had suggested that silicate signatures were muted or missing in periodic comets and that new comets usually have strong 10- and 20-μm emission features indicating the presence of small silicate grains, the additional data we present here leads to the conclusion that the presence or absence of small silicate grains does not necessarily depend upon the processing history of the nucleus. Indeed, as shown in Fig. 2, the old Comet P/Halley has stronger silicate emission than any of the new comets in our sample, and there are at least two examples of new comets (KBM and Austin 1984) that have no small silicate grain component. The superheat of the continuum emission from these last two is quite small, suggesting that they have large grains like the anti-tail of Comet Kohoutek (Fig. 1); the grains in this case may be larger than hundreds of micrometers. Telesco *et al.* (1986) have concluded that the dust tail of Comet Giacobini–Zinner was composed of dust grains with radii as large as $\approx$300 μm. In the case of the comets with optically thin silicate emission features, the super heat is high enough to signify that grains with radii as small as

TABLE IV
Mean Properties of Selected Bright Comets[1]

NAME	SPECIAL SELECTION CRITERIA, COMMENTS	SILICATE EMISSION EXCESS IN MAGNITUDES	%S (<S>-1 X100)
1975 IX	Extreme IR Type I Comet	0.18 ± 0.03	5 ± 1
1980 XV	IR Type I Comet	0.33 ± 0.07	11 ± 2
1984 XIII	Extreme IR Type I Comet	0.13 ± 0.03	5 ± 2
1985 VIII	IR Type I Comet	0.25	7
1989c$_1$	IR Type I Comet	0.20 ± 0.08	7 ± 6
1989 X	IR Type I Comet	0.11 ± 0.11	6 ± 3
Bennett	Extreme IR Type II Comet	1.08 ± 0.11	37 ± 9
Kohoutek	IR Type II Comet	0.68 ± 0.11	22 ± 3
West	IR Type II Comet	0.66 ± 0.10	34 ± 7
IR Type I	Average over all IR Type Comets above	0.24 ± 0.03	8 ± 1
IR Type II	Average over all IR Type II's above	0.76 ± 0.08	29 ± 3
P/Halley	Average of all days	0.53 ± 0.04	27 ± 1

[1] The errors quoted here are the standard deviation of the mean σ_x, of all measurements of a given comet, or grouping of comets.

0.5 to 1 μm dominate the emission from the center of the coma.

A key issue is whether the continuum emission and the silicate emission features are from separate grain distributions, or whether both spectral components are emitted by composite, fluffy aggregate grains having either the "cluster-of-grapes" morphology exhibited by interplanetary dust particles (IDPs) collected in the atmosphere and oceans of the Earth (Brownlee 1987, Brownlee *et al.* 1980, Fraundorf *et al.* 1982) or the core/mantle structure as proposed by Hanner *et al.* (1981), Greenberg (1982, 1986), and Greenberg and Hage (1990). Gehrz *et al.* (1989) have argued that the presence or absence of the 10- and 20-μm emission features can be explained by grain size effects alone. We present evidence in the discussion below that our albedo measurements and the correlation between superheat and 10-μm silicate emission strength (Table IV, Fig. 6) appear to favor the composite grain hypothesis.

Superheat as a grain size indicator. P/Halley and other IR Type II comets are characterized by an elevation of the temperature of the thermal infrared continuum considerably above the black-sphere temperature appropriate to the comet's heliocentric distance. Ney (1974a, 1982a) has suggested that the grains in these comets are superheated because they are too small to radiate like blackbodies. A quantitative measure of the relationship between the grain radius and the grain temperature T_{gr} can be established by setting the power absorbed by the grain from the solar radiation field equal to the power emitted by the grain in the thermal infrared,

$$\frac{L_\odot}{4\pi r^2}\pi a^2 Q_a = 4\pi a^2 Q_e \sigma T_{gr}^4, \tag{1}$$

where r is the heliocentric distance, a is the grain radius in centimeters, $L_\odot = 3.826 \times 10^{33}$ erg sec^{-1} is the solar luminosity, $\sigma = 5.6696 \times 10^{-5}$ erg cm^{-2} deg^{-4} is the Stefan–Boltzmann constant, and $Q_a(a, T)$ and $Q_e(a, T)$ are the Planck mean absorption and emission coefficients (see Gilman 1974). Q_a is the absorption efficiency of the grain averaged over the energy distribution of the illuminating source (the Sun), and Q_e is the thermal emission efficiency of the grain at T_{gr}. Solving Eq. (1) for the grain temperature yields

$$T_{gr} = \left[\frac{L_\odot Q_a}{16\pi\sigma r^2 Q_e}\right]^{1/4}, \tag{2}$$

which gives the black sphere temperature T_{BB},

$$T_{BB} = \frac{278}{\sqrt{r_A}}\text{K}, \tag{3}$$

in the case when $Q_a = Q_e = 1$, where r_A is the heliocentric distance in AU (1 AU = 1.4960×10^{13} cm). Equation (2) demonstrates that for small grains where $Q_e < Q_a$, the grain temperature must rise above the black-sphere temperature in order for the grain to come to radiative equilibrium. Equation (3) defines a lower limit to the temperature that comet grains can assume as a function of heliocentric distance.

We define the superheat $S = T_{obs}/T_{BB}$ as the ratio of the observed carbon-grain temperature to that expected for a perfectly conducting black sphere at the same heliocentric distance. Assuming that the infrared color temperature of the grains T_{obs} measures the physical temperature of the grain T_{gr}, Eqs. (2) and (3) can be combined to show that S measures the fourth root of the ratio of Q_a to Q_e,

$$S = \frac{T_{obs}}{T_{BB}} = \left[\frac{Q_a}{Q_e}\right]^{1/4}, \tag{4}$$

where the right-hand side is unity for large grains and becomes progressively larger as the grain size decreases. T_{obs} and T_{gr} are equivalent in cases where the grain emissivity does not vary significantly over the spectral region used to define the color temperature. Our determination of the carbon continuum color temperature was heavily weighted by measurements in the 2.3- to 8.7-μm spectral region where the emissivity is approximately constant for small carbon grains with radii larger than about 0.5 μm (see Temi *et al.* 1989), and we believe that the color tem-

peratures given in column 9 of Table III are representative of the physical grain temperatures. Some comets, including P/Halley, show weak hydrocarbon emission at 3.28 μm (Brooke *et al.* 1986, 1988, 1991), and silicates can contribute weakly to the 8.6-μm emission. Neither of these emission contributions significantly affects the continuum color temperature for the cases studied here.

We calculated the superheat as a function of grain radius a and temperature T_{gr} for small carbon grains illuminated by the solar radiation field using the Planck mean absorption cross sections for graphite grains published by Gilman (1974). The Sun was assumed to radiate like a blackbody with an effective temperature of 5800 K. Our results are plotted in Figs. 4–6.

The dependence of the grain temperature on heliocentric distance (Fig. 4) shows that the grains in P/Halley (Fig. 4b) were superheated compared to those in the remaining comets in this survey (Fig. 4a). In both cases, it is evident that the grain temperature falls as the square root of the heliocentric distance. All of the comets plotted in Fig. 4a are IR Type I, which have relatively large grains. We believe that the comparison of various comets presented in Fig. 4c provides a powerful demonstration that Eq. (3) defines the lower limit to the temperature of comet dust. The comet dust trails detected by the Infrared Astronomical Satellite IRAS (Sykes *et al.* 1986, Sykes and Walker 1992) and the anti-tail of Comet Kohoutek (Ney 1974a) are included in the summary comparison presented in Fig. 4c. The particles in comet dust trails and Kohoutek's anti-tail are expected to be large compared to the grains in the inner coma, and they therefore provide an excellent indication of the lowest temperatures that can be attained by cometary solids.

The cross-hatched region in Fig. 5 shows the range of grain temperatures and superheats recorded for P/Halley (Table III). We conclude that P/Halley's coma continuum emission was usually produced by grains with radii between 0.5 and 1 μm. There were occasional episodes when P/Halley's grains appeared to be as large as 5 μm (Fig. 5). It is apparent from Fig. 5 that grains larger than 6–7 μm probably populate the comae of the average IR Type I comet.

An examination of similar data on the thermal emission from other extreme IR Type II comets (Maas *et al.* 1970, Ney 1974a,b, 1982a) leads us to conclude that their comae have small grains similar to those in the coma of P/Halley. On the other hand, the thermal emission from the comae of the most extreme IR Type I comets observed in the current study appears from Table III and Fig. 5 to be predominantly from large grains. The superheat in Comets KBM, Bradfield 1980 XV, Austin 1984 XIII, and Austin 1989c$_1$ was frequently low enough to imply that the coma grains were as large as 20 μm. The absence of strong silicate emission in the IR Type I comets (Fig. 2b) may also indicate the presence of large silicate grains. Ordinarily, the absence of the 10-μm silicate emission feature is taken to indicate that the grains are carbon or iron. However, Rose (1979) reported laboratory experiments demonstrating that olivine grains with radii $\approx$10–20 μm had weak 10-μm emission features and that grains larger than 37 μm exhibited no feature at all.

Although there is no reason to believe a priori that the size distributions of the carbon and silicate grains in comets are related, our data show that there is a fairly strong correlation between superheat and 10-μm silicate emission excess (Table IV and Fig. 6), with silicate emission increasing as superheat increases. Ney (1982a) noted a similar tendency among a smaller sample of comets. Several interpretations of this result appear plausible. It is possible that the grain-size distributions of the carbon and silicate particles are quite similar, so that the processes that apparently deplete the small particles in the IR Type I comets affect both types of particle similarly. Alternatively, the comet grains may be highly irregular fluffy aggregates of silicate and carbonaceous grains. Two possible forms for these aggregates are the "cluster-of-grapes" morphology exhibited by the IDPs described by Brownlee (1987), Brownlee *et al.* (1980), and Fraundorf *et al.* (1982) and the silicate–core/carbon–mantle particles suggested by Greenberg (1982, 1986). In the case of aggregate particles, both the continuum emission and the silicate emission arise from the same particles, and increasing particle size naturally leads to a suppression of both the superheat and the silicate emission feature (see the discussion of the large grains in Comet P/Encke by Gehrz *et al.* 1989). Both scenarios require that the IR Type I comets be relatively depleted of small particles.

We have plotted values averaged over all measurements of each comet in Fig. 6. Despite the strong correlation between superheat and silicate excess, there were occasional episodes for some comets when low superheat was accompanied by strong silicate emission (e.g., Bradfield 1980 XV, Days +3.3 and 4.3), and vice versa (e.g., Austin 1989c$_1$, Day +5.82). There may be conditions under which the carbon and silicate components can be affected independently.

The albedo of comet dust and the structure of the grains. Following the arguments presented by Van de Hulst (1957), Hanner *et al.* (1981), and Eaton (1984), we define a bolometric albedo A for small grains by the relationship

$$\frac{f_{\rm vis}}{f_{\rm IR}} = \frac{A}{1 - A}, \tag{5}$$

where the left-hand side of Eq. (5) is the ratio of the energy scattered in all directions to the total energy removed

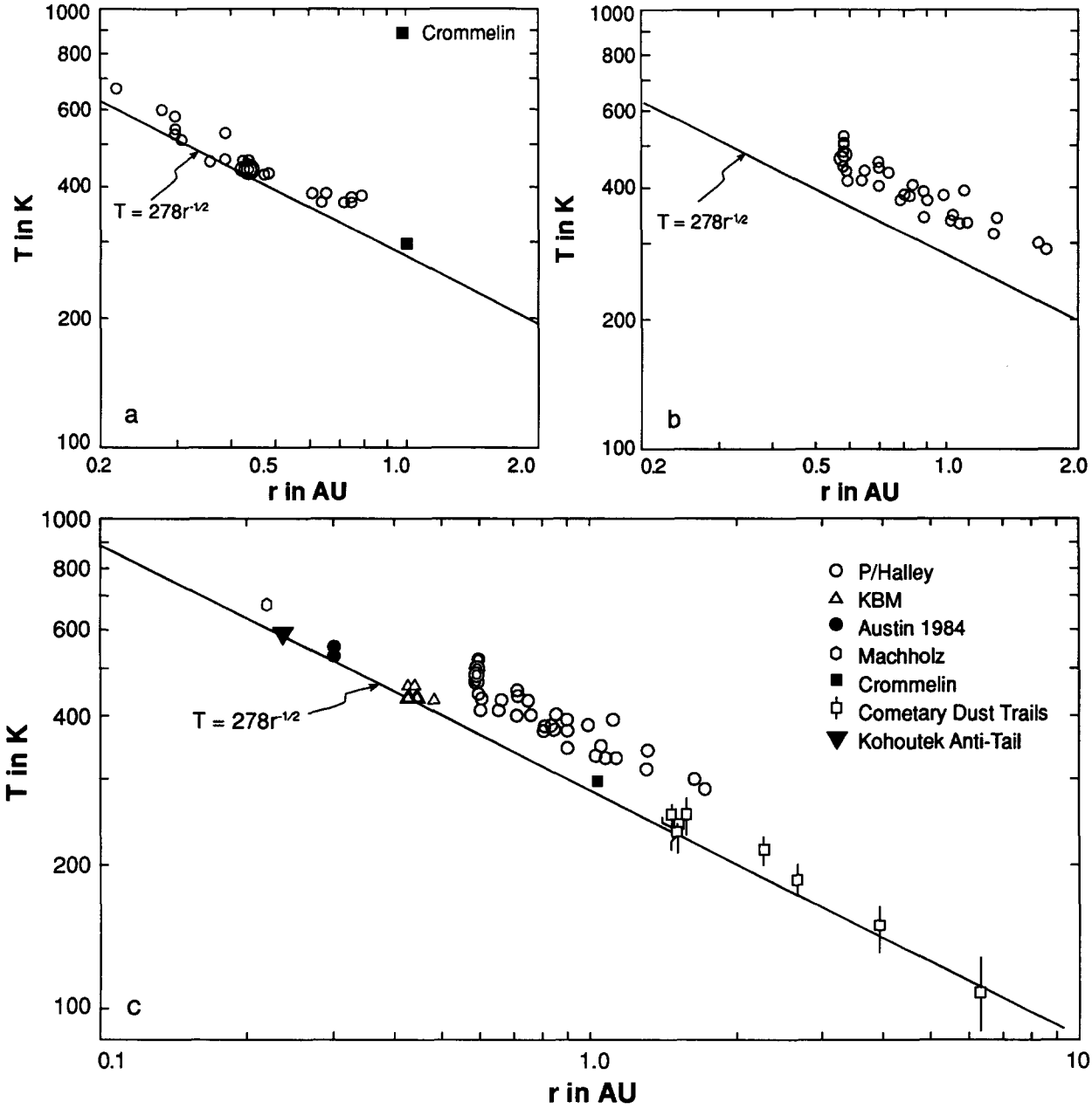

FIG. 4. The observed coma continuum temperature T_{obs} plotted as a function of heliocentric distance for (a) the six comparison IR Type I comets observed in the present survey (open circles) and comet Crommelin 1983n (datum from Hanner *et al.* 1985b), (b) Comet P/Halley, and (c) Comet P/Halley compared with the IR Type I comets with the lowest superheat from this survey, Comet Crommelin 1983n, the anti-tail of Comet Kohoutek, and the cometary dust trails detected by the Infrared Astronomical Satellite IRAS (data from Sykes and Walker 1992). Crommelin 1983n is the darkest comet known. The comet dust trails detected by IRAS (Sykes *et al.* 1986, Sykes and Walker 1992) and the anti-tail of Comet Kohoutek (Ney 1974a) shown in panel (c) are believed to be composed of large particles and therefore provide an indication of the lowest temperatures that can be attained by cometary solids. The solid line given by Eq. (3) evidently sets the lower limit to the temperature that comet grains assume as a function of heliocentric distance. It is apparent that P/Halley shows a much larger temperature excess on the average than do the comparison comets. In both cases, the data are consistent with an $r^{-1/2}$ dependence for the temperature.

from the incident beam, f_{vis} is the apparent intensity integrated over all scattering angles due to scattering of solar radiation, and f_{IR} is the integrated apparent thermal emission due to reradiation of the absorbed component. In the case of small comet grains, the quantity in the numerator of the left-hand side of Eq. (5) must be derived from measurements of the visible/near-infrared energy distribution of the coma at all phase angles, because the scattering phase function is highly anisotropic (see Van de Hulst 1957, Bohren and Hufmann 1983, Hanner *et al.* 1981).

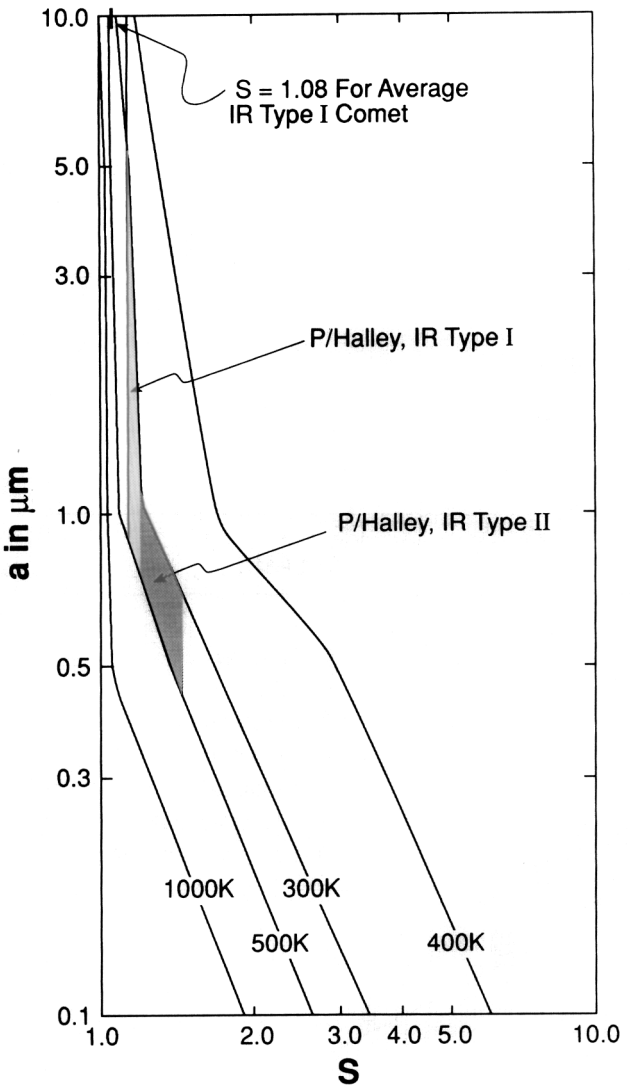

FIG. 5. The superheat S plotted as a function of grain radius a and temperature T_{gr} for small carbon grains illuminated by the solar radiation field, assuming that the Sun has an effective temperature of 5800 K. Curves are based on Gilman's (1974) calculations of the Planck mean absorption cross sections for graphite grains. The range of grain temperatures and superheats recorded for P/Halley confirm that its coma continuum emission was usually produced primarily by particles with radii between 0.5 and 1 micrometer. When P/Halley exhibited IR Type I characteristics, its coma grains may have been as large as 5 μm. Typical IR Type I comets as characterized by the remaining comets in this survey have an average superheat of $S = 1.08$, suggesting the presence of grains with radii as large as 10 μm.

Since the energy removed from the beam is that absorbed by the grains and therefore reemitted by them in the infrared, the quantity in the denominator can be determined by measurements of the thermal infrared energy distribution of the coma. For a scattering angle θ, the bolometric albedo as a function of scattering angle $A(\theta)$ given by the integrated scattered and emitted energy distributions follows from Eq. (5) as

$$A(\theta) = \frac{f(\theta)}{1 + f(\theta)}, \tag{6}$$

where

$$f(\theta) = \frac{f_{\rm vis}(\theta)}{f_{\rm IR}(\theta)} = \frac{[\lambda f_\lambda(\text{vis}, \theta)]_{\max}}{[\lambda f_\lambda(\text{IR}, \theta)]_{\max}}. \tag{7}$$

In Eq. (7), $f_{\rm vis}(\theta)$ and $f_{\rm IR}(\theta)$ are the integrated apparent intensities in the scattered and thermal energy distributions of the coma, respectively, for the scattering angle θ.

The mean bolometric albedo A averaged over all scattering angles is then given by

$$A = \frac{1}{\pi}\int_0^\pi A(\theta)\, d\theta. \tag{8}$$

The scattered and thermal energy distributions of comets can be closely approximated by blackbody energy distributions. We show in Appendix A that, for black body radiation, the integrated intensity F is related to the maximum of the (λF_λ) function by $F \approx 1.36(\lambda F_\lambda)_{\max}$. The quantities $[\lambda f_\lambda(\text{vis})]_{\max}$ and $[\lambda f_\lambda(\text{IR})]_{\max}$ for P/Halley are plotted as a function of r in Fig. 7.

We have examined the scattering phase function of comet grains for a number of comets by measuring the ratio of the solar energy reflected by the grains to the absorbed solar energy reemitted by the grains as a function of phase angle (Fig. 8). Comets West 1976 VI (1975h) (Ney and Merrill 1976) and Bradfield 1980 XV (Tables I–III) passed between the Earth and the Sun, enabling us to make an excellent determination of $A(\theta)$ for typical comet grains at scattering angles between 30° and 150° (Fig. 8a). Our observations of these comets near inferior conjunction showed that typical comet grains have a moderately strong forward-scattering peak as would be expected for small particles (Fig. 8b). There is no evidence in our comet data for a backscattering peak that would be expected for spherical particles (Fig. 8b), and the forward-scattering lobe for comet dust is lower than that expected for spherical particles (Fig. 8b). Typical comet grains as defined by the data on Comets West and Bradfield 1980 XV have a mean bolometric albedo of $A \approx 0.32$, and $A(\theta) \approx 0.15$ for scattering angles between 120° and 180°.

The flattened forward-scattering lobe and the absence of a pronounced backscattering peak in $A(\theta)$ for comet dust (Fig. 8a) strongly suggest that the comet grains are nonspherical and, perhaps, fluffy aggregates as suggested by Hanner *et al.* (1981), Greenberg (1982, 1986), Greenberg and Hage (1989). Figure 8b shows $A(\theta)$ derived from laboratory data for small cloud chamber droplets (from the data presented by Webb 1935 and Wilson 1951), nonspherical particles (Bohren and Hufmann 1983), and

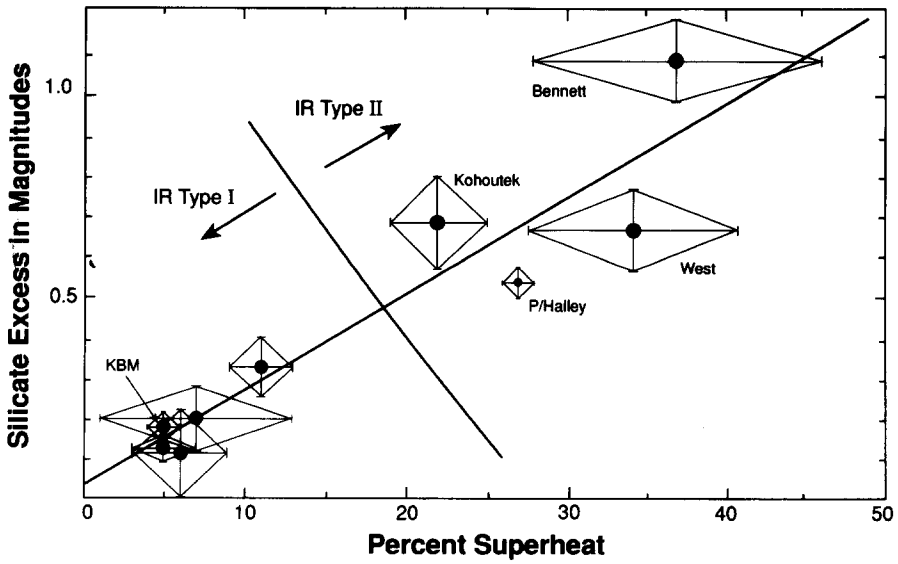

FIG. 6. The silicate excess (in magnitudes) plotted as a function of percent superheat ($[S - 1] \times 100$; see Eq. (4) for the definition of S) for recent bright comets (data in Table IV). The linear relation (solid line) is $y = 0.0233x + 0.0394$. The correlation coefficient is 0.94.

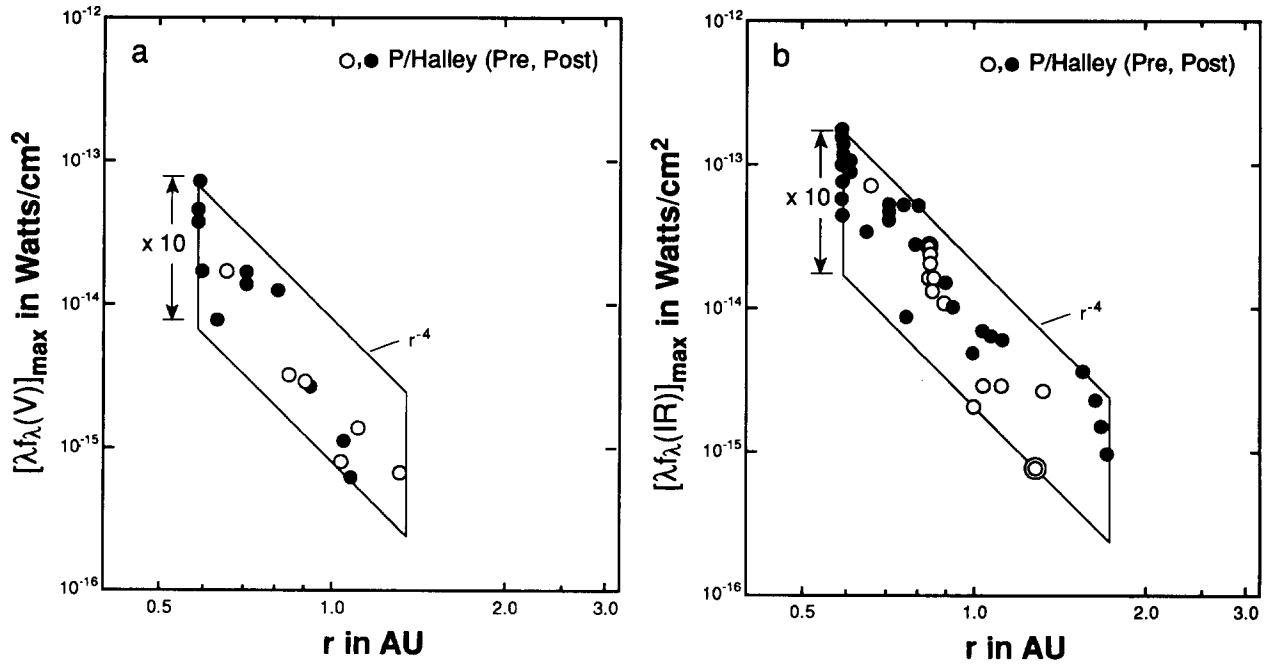

FIG. 7. The activity of the nucleus of P/Halley as a function of heliocentric distance at (a) visible and (b) infrared wavelengths as measured by variations of the apparent intensities $[\lambda f_\lambda(V)]_{max}$ and $[\lambda f_\lambda(\mathrm{IR})]_{max}$, respectively. The coma model described in Appendix A has been used to correct the data for emission in the reference beam and to normalize the apparent intensities to a geocentric distance of $\Delta = 1$ AU and a beam diameter of 20 arcsec. Statistical errors are smaller than the plotting symbols. The parallelograms superimposed on panels (a) and (b) show that P/Halley generally brightened proportionally to r^{-4} as predicted by the theory of nuclear activity described by Eqs. (9) through (12), but varied by almost a factor of 10 on short time scales.

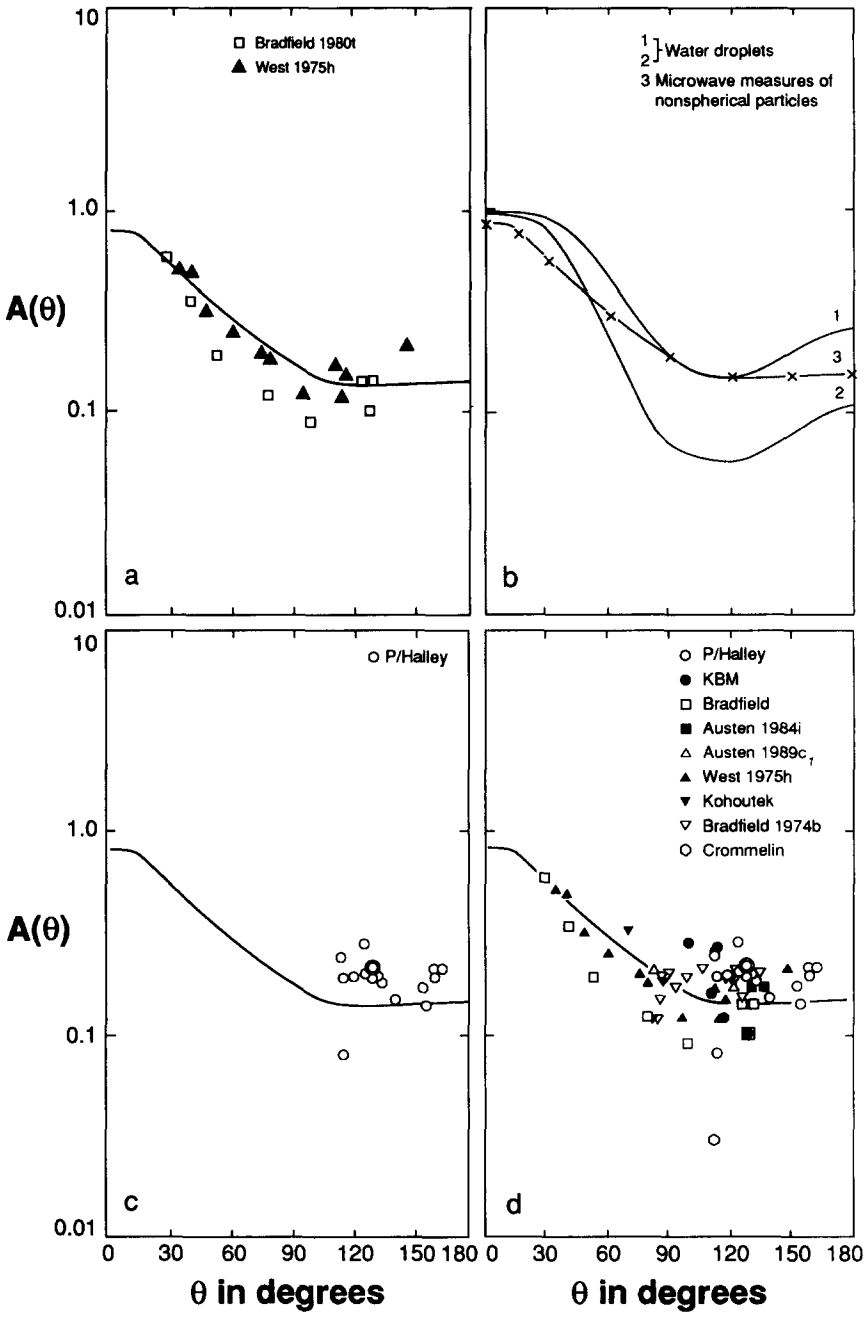

FIG. 8. The albedo of comet grains as a function of scattering angle as measured by the ratio of the scattered to the reemitted (absorbed) radiation. Panel (a) shows data for West 1975h (data for Ney and Merrill 1976) and Bradfield 1980 XV (data from this paper) that define the albedo of cometary grains for scattering angles between 30° and 150°. The flattened forward scattering lobe and the absence of a pronounced backscattering peak suggest that the comet grains are nonspherical and, perhaps, fluffy. Panel (b) shows laboratory data for small water droplets in cloud chambers (from the data presented by Webb 1935 and Wilson 1951) and nonspherical particles (Bohren and Hufmann 1983, Hanner *et al.* 1981). Panel (c) shows data for P/Halley for scattering angles between 114° and 165°, illustrating that P/Halley's grains were highly variable in albedo, but on the average were about the same as the grains of the comets in panel (a). Panel (d) shows data for Comet West 1975h (data from Ney and Merrill 1976), Crommelin 1983n (datum from Hanner *et al.* 1985b), and all the comets for which new data are reported in this paper with curve 3 from Fig. 5b superimposed for comparison. The side scattering albedo of comet grains generally lies in the range $0.1 \leq A \leq 0.3$, and the grains of individual comets can display a high degree of variability in albedo. To our knowledge, Crommelin is the darkest comet on record.

fluffy aggregates (Hanner *et al.* 1981). The comet data are consistent with the curves for nonspherical particles and fluffy aggregates. These characteristics are also consistent with theoretical results for "fluffy" aggregates (Greenberg 1982, 1986).

Figure 8c shows $A(\theta)$ for P/Halley for scattering angles between 114° and 165°, indicating that P/Halley's grains were highly variable in albedo, but on the average had a side-scattering albedo similar to that of the grains of the comets in Fig. 8a. We were able to observe P/Halley at backscattering angles out to 165° near perihelion passage. Any backscattering increase appeared to be small. P/Halley's dust coma had an average albedo of $A(\theta) \approx 0.20$ at a scattering angle of 130°, making it slightly brighter than the comae of average comets at phase angles from 120° to 165°. This would be expected for an extreme IR Type II comet with a significant small silicate grain component. We note that the lowest side-scattering albedo we observed for P/Halley ($A(\theta) \approx 0.08$) occurred when the 10-μm silicate emission feature was absent. Both of these indicators are consistent with a coma at these times that was populated predominantly by large grains.

Figure 8d shows $A(\theta)$ for Comet West, Comet Crommelin 1983n, and all the comets for which data are reported in this paper. We conclude that the side-scattering albedo of comet grains generally lies in the range $0.1 \leq A \leq 0.3$, but that the grains of individual comets can display a high degree of temporal variability in albedo during an apparition.

Variations in the silicate emission feature and albedo. Variations in several grain composition indicators were observed for P/Halley. Our data (Fig. 3) and additional infrared data obtained by Hanner *et al.* (1987) and Tokunaga *et al.* (1986 and 1988) at the NASA Infrared Telescope Facility (IRTF) show that P/Halley's silicate emission feature was occasionally weak or absent. Although this behavior usually occurred at heliocentric distances greater than 1 AU, there were several occasions when this behavior occurred at small heliocentric distances (e.g., 26.8 January 1986 UT and 14.67 February 1986 UT). Furthermore, our data show that the strength of the 10-μm silicate emission feature varied significantly when P/Halley was inside a heliocentric distance of 1 AU (Fig. 3). Ryan and Campins (1991) reached a similar conclusion based upon a more limited data set.

The disappearance of the silicate signature for distances greater than 1 AU was previously noted for Comet Kohoutek by Rieke *et al.* (1974). Comet Bradfield 1980 XV (Ney 1982a and Tables I–III of this paper) clearly was an IR Type II comet near perihelion (Fig. 2a), but showed no silicate emission beyond $r = 0.6$ AU.

On one occasion when P/Halley's silicate feature was missing, the dust albedo fell as low as 0.08 (Fig. 8). A similar correlation between silicate signature strength and dust albedo is clearly evident for Comet Bradfield 1980 XV (this paper, Table III) and was noted in Comet Bradfield 1974b by Ney (1974b).

C. The Physics of the Nuclear Ablation Process

Our observations provide information about the nature of the nuclear ablation process by (i) showing that production rate and outflow of grains from the nucleus nominally conforms with the steady-state model, (ii) establishing the amplitude of short-term temporal variations in the activity of the nucleus, and (iii) measuring the mass loss rate of the solid material.

Constraints on models of the production and outflow of coma grains. We made nearly simultaneous observations of P/Halley with several diaphragms on four separate occasions using the O'Brien and WIRO telescopes and obtained multiaperture photometry of Comet Bradfield 1980 XV during a time span of about 1 hr on one occasion from Wyoming. These multiaperture measurements can be interpreted in terms of the steady-state model of nuclear activity described in Appendix B. In this model, grains are released from the nucleus at a constant rate and flow outward from the nucleus at constant velocity. Reitsema *et al.* (1989), in an elegant study, showed that the visible images of the inner coma of P/Halley by *Giotto* were consistent with the interpretation that the individual active areas on the nucleus behave according to the steady-state model.

Our multidiaphragm observations of P/Halley and Comet Bradfield 1980 XV (Fig. 9) show that the coma flux was usually proportional to ϕ and that the steady-state grain production model was valid for times as great as 0.25 days (6 hr) on most occasions. Possible jet-like activity developing rapidly on time scales of a few hours is suggested by our P/Halley observations on 9.83 February 1986 UT, when the average flux recorded in a 20-arcsec beam at O'Brien was less than that expected from the flux recorded in an 8.3-arcsec beam at WIRO. The sudden activation of an intense gas jet, similar to those seen in the *Giotto* images (Keller *et al.* 1986), appears to provide a plausible explanation for the 9.83 February measurements. One set of infrared imaging observations, obtained a few hours prior to the *Giotto* encounter by Hayward *et al.* (1986), tends to confirm the hypothesis that the infrared variations may be profoundly affected by jets releasing material on the sunward side of the nucleus.

Activity in comet nuclei. Figures 7 and 10 summarize the activity of the nuclei of P/Halley and the six other recent bright comets studied in this work as measured by the infrared luminosities of their comae. In Fig. 10, we have included schematic representations of the average

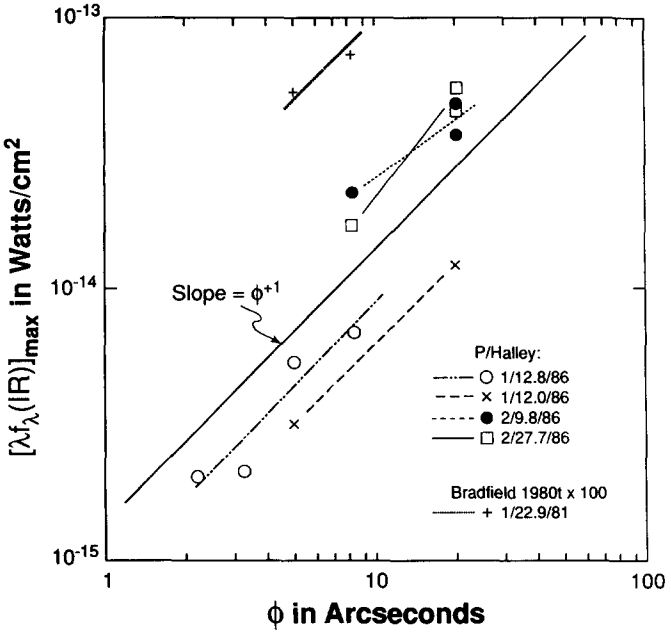

FIG. 9. Coma brightnesses of P/Halley and Bradfield 1980 XV as a function of aperture diameter. The coma model described in Appendix A has been used to correct the data for emission in the reference beam. The data are generally consistent with a constant production rate of grains in a constant velocity outflow (the steady-state model described in Appendix A).

activity of some of the other bright comets we have measured previously (Ney 1982a, Gehrz *et al.* 1989). The activity in most comets is proportional to r^{-4} both preceding and following perihelion passage with small superimposed variations. Comet West 1976 VI (1975h) brightened significantly after perihelion because the nucleus broke into four parts. Encke probably behaves differently than most comets because of an appreciable contribution to the thermal emission by the nucleus itself (Gehrz *et al.* 1989).

The apparent infrared intensity $f_\phi(\mathrm{IR})$ of an optically thin comet coma in a beam of angular diameter ϕ radians that is much smaller than the angular extent of the coma follows from Eqs. (2), (A-4), and (A-6), to be

$$f_\phi(\mathrm{IR}) = 1.3586(\lambda f_\lambda)_{\max} = \left[\frac{\pi a^2 Q_e \sigma T_{obs}^4}{4V_0}\right]\frac{\phi}{\Delta}\frac{dN}{dt} = \left[\frac{a^2 Q_a L_\odot}{64V_0}\right]\frac{\phi}{r^2\Delta}\frac{dN}{dt}, \quad (9)$$

where Q_a and Q_e are, respectively, the Planck mean absorption and emission coefficients for the grains as defined by Gilman (1974), where r and Δ are the heliocentric and geocentric distances in centimeters. If the grain production rate as a function of heliocentric distance $dN(r)/dt$ is directly proportional to the intensity of the solar radiation incident upon the nucleus, then

$$\frac{dN(r)}{dt} = \frac{dN(r_p)}{dt}\left[\frac{r_p}{r}\right]^2, \quad (10)$$

where r_p is the perihelion distance, $dN(r_p)/dt$ is the grain production rate in grains sec^{-1} at perihelion, and r is the heliocentric distance. Combining Eqs. (9) and (10), we find that the apparent coma intensity is

$$f_\phi(\mathrm{IR}) = \left[\frac{a^2 Q_a L_\odot}{64V_0}\right]\frac{\phi}{r^4\Delta}\frac{dN(r_p)}{dt} \propto \frac{\phi}{r^4\Delta}. \quad (11)$$

An interesting variation of the relationship expressed by Eq. (11) occurs in the case when the luminosity of the coma is generated by emission from small silicate grains for which the emission efficiency is proportional to the grain radius a (Gilman 1974). In this case, the apparent infrared intensity of the coma is directly proportional to the total mass M_{gr} of the grains,

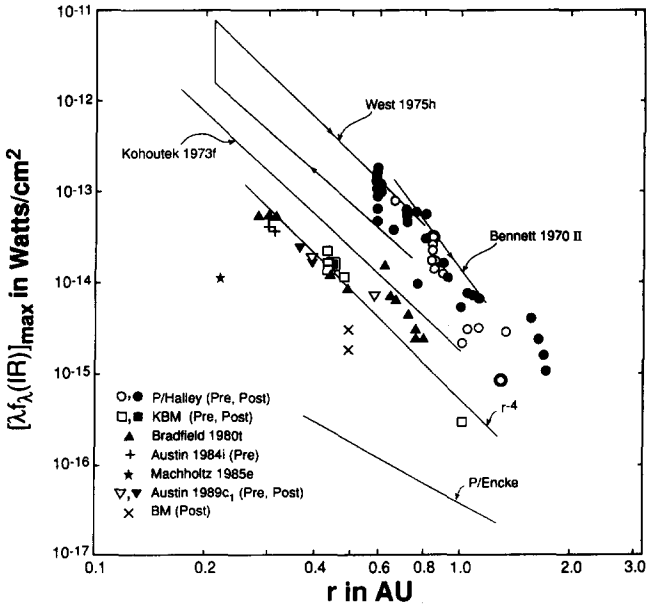

FIG. 10. The infrared activity of the nucleus of P/Halley compared to that of the nuclei of other recent bright comets as a function of heliocentric distance as measured by variations in the quantity $[\lambda f_\lambda(\mathrm{IR})]_{max}$. The coma model described in Appendix A has been used to correct the data for emission in the reference beam and to normalize the apparent intensities to a geocentric distance of Δ = 1 AU and a beam diameter of 20 arcsec. Comets Bennett 1970 II, Kohoutek 1973f, West 1975h (Ney 1982a), and P/Encke (Gehrz *et al.* 1987) are shown for comparison; the step function in activity for West near perihelion was caused by the breakup of the nucleus. An r^{-4} activity model adequately describes the heliocentric brightening of almost all comets. P/Halley exhibited large variations about the canonical law.

$$f_\phi(\mathrm{IR}) \propto \frac{M_{gr}\phi}{r^4\Delta}. \quad (12)$$

It is evident from Eq. (11) that the approximation quantified in Eq. (10) for the apparent luminosity of comets implies a dependence of r^{-4} for both the energy absorbed and the energy reemitted. The quantity $(\lambda f_\lambda)_{max}$ for the thermal emission is a measure of the energy reradiated and is equal to the energy absorbed. It is a better measure of a comet's intrinsic brightness than short-wavelength reflected light measurements because of the variation in albedo with phase angle.

Both short-term and long-term variations in comet nucleus activity that are superimposed upon the r^{-4} radial dependence can be readily evaluated by examination of the quantity given in column 18 of Table III. This quantity has been normalized using Eqs. (11), (B-1), and (B-2) to give the flux expected in a standard circular 20-arcsec diameter diaphragm for an infinite reference beam throw with the comet at a standard heliocentric distance of r = 1 AU and a standard geocentric distance of Δ = 1 AU.

In the comparison with the six other comets observed in this work (Fig. 10), P/Halley (Fig. 7) is seen to exhibit more frequent large-amplitude variations about the r^{-4} brightening law than is usually the case. Overall, we found that P/Halley varied in brightness by a factor of up to 7 on time scales of a few hours and days and by a factor of 10 overall compared to the expected rate of brightening with changing heliocentric distance; its thermal emission was as dim on some occasions as that of Kohoutek 1973f and as bright as that of Comets Bennett 1970 II and West 1975h on others. The large variations of P/Halley are also apparent in the scattered component (Fig. 7).

Our data enable us to draw several conclusions with regard to the activity of the nucleus and coma of P/Halley:

(1) Neither the large short-term variations nor the long-term variations in the bolometric infrared emission from P/Halley appear to correlate in any detail with the visible variations reported by Green and Morris (1987) and Millis and Schleicher (1986). Green and Morris (1987) found that the heliocentric dependence of the integrated visible magnitude of P/Halley's coma varied asymmetrically about perihelion passage, with the comet being significantly brighter postperihelion. Our data show that both the heliocentric dependence of the scattered light (Fig. 7a) and the thermal emission within a 20-arcsec beam were comparable pre- and postperihelion. Both our data and those of Green and Morris show large-amplitude short-term variations, but there is no detailed correlation between the intensity variations seen in our small beam with those exhibited by the entire coma.

(2) Millis and Schleicher (1986) and Schleicher *et al.* (1990) reported visual photometry showing periodic variations on a time scale of 7.4 days that they attributed to activity associated with the illumination of different regions of the nucleus. Although there is no obvious tight correlation between the variations exhibited in our data and those reported during overlapping periods by Millis and Schleicher (1986), both our data sets appear to be consistent with the inner coma being fainter in visible emission around 20 March 1986 and brighter around March 15, 23, and 25.5. We conclude that our data are consistent with the interpretation that the infrared variations in P/Halley result from rotation of the nucleus, presenting active and passive surfaces to the Sun. Both *Giotto* images (Keller *et al.* 1986) and the groundbased 10-μm infrared images made during the *Giotto* passage by Hayward *et al.* (1986) suggest the presence of localized active jets on P/Halley's nucleus which could account for such behavior.

(3) McFadden *et al.* (1987) and Rettig *et al.* (1987) noted a marked brightening of P/Halley in several visible emission bands during 23–25 March 1986 UT. Our data do not show any conclusive evidence of unusual brightening in either the scattered or the thermal emission from the inner 20 arcsec of the coma at the beginning and end of this period.

Dust mass loss rates of comet nuclei. The dust mass loss rate dM_D/dt caused by the ablation of dN/dt grains sec^{-1} from the comet nucleus, each having density ρ_{gr} and radius a, is

$$\frac{dM_D}{dt} = m_{gr}\frac{dN}{dt} = \frac{4\pi}{3}\rho_{gr}a^3\frac{dN}{dt}, \quad (13)$$

where m_{gr} is the mass of a single grain. Combining Eqs. (9) and (13), we find that

$$\frac{dM_D}{dt} = [1.3586(\lambda f_\lambda)_{max}]\frac{256\pi}{3}\frac{a\rho_{gr}}{L_\odot Q_a}V_0\frac{r^2\Delta}{\phi}, \quad (14)$$

where V_0 is the grain ejection velocity and $(\lambda f_\lambda)_{max}$ is obtained by correcting the intensity given in Table III, column 11, for beam throw effects using Eq. (B-1). Presuming that the grains are accelerated to terminal velocity by momentum coupling to the gas, V_0 is of the order of the sonic velocity in the gas (Finson and Probstein 1968) which is given with the aid of Eq. (3) by

$$V_0 = 5\times10^4\left[\frac{T_{bb}}{278}\right]^{1/2} = \frac{5\times10^4}{r_A^{1/4}}\ \mathrm{cm\ sec^{-1}} \approx 0.5\ \mathrm{km\ sec^{-1}}, \quad (15)$$

where T_{BB} is the blackbody temperature at the heliocentric

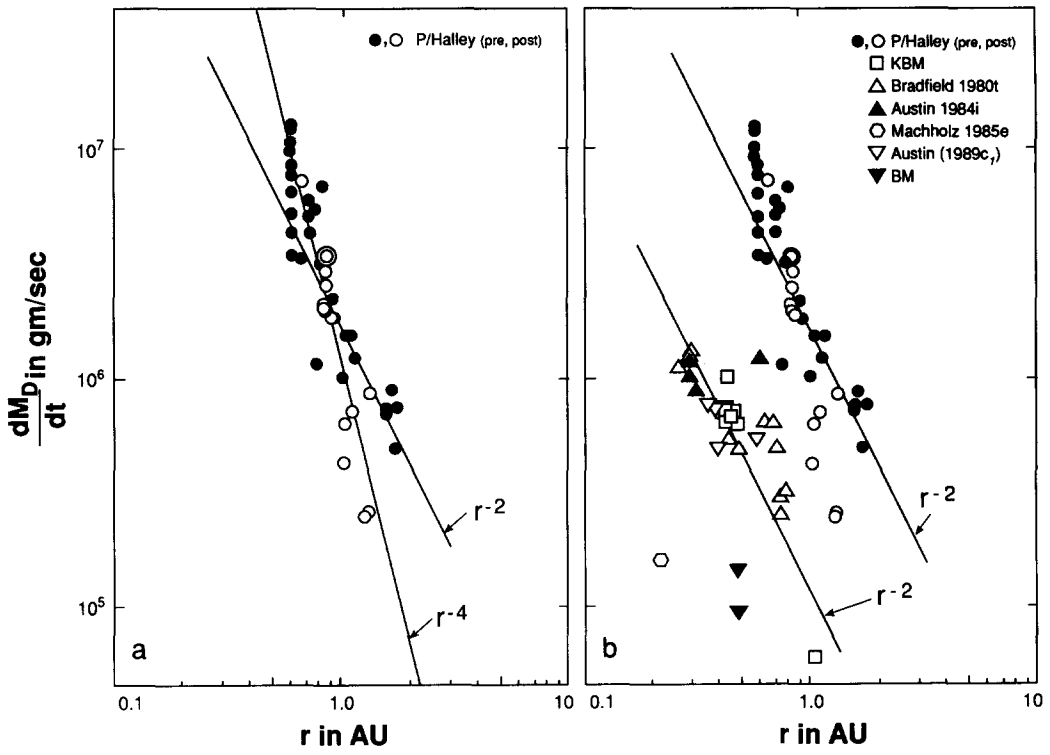

FIG. 11. The dust mass loss rates (normalized to a grain radius of 1 μm and a geocentric distance of Δ = 1 AU) as a function of heliocentric distance (a) from the nucleus of P/Halley and (b) from the nucleus of P/Halley in comparison with the nuclei of the IR Type I comets in this survey. The coma model described in Appendix A has been used to correct the data for emission in the reference beam and to normalize the apparent intensities to a geocentric distance of Δ = 1 AU and a beam diameter of 20 arcsec. P/Halley showed substantial bursts of activity superimposed on the canonical r^{-2} law. The dust mass loss rates of the IR Type I comets shown here may be multiplied by a factor of 10 if it is presumed that their comae are composed primarily of 10 μm grains. In this case, their dust mass loss rates are equivalent to the rates inferred for dusty IR Type II comets like P/Halley.

distance r_A in AU of the comet. Given the very weak dependence of V_0 on r, we use the approximation that $V_0 \approx 0.5$ km sec^{-1} in the analysis that follows. We concluded above that the observed superheat S for the IR Type II comets discussed herein suggests a typical grain radius of $a \approx 1$ μm $= 10^{-4}$ cm for the carbon grains responsible for the continuum emission. Typical IDP aggregates have a density of ≤ 1 g cm^{-3}, while pure carbon and silicate grains would have densities of ≈ 2–3 g cm^{-3}. We conclude that a typical comet grain can be presumed to have a density of ≈ 1 g cm^{-3} (see also Hanner 1988). Using Eqs. (14) and (15) with a = 1 μm, ρ_{gr} = 1 g cm^{-3}, and Q_a = 1, the dust mass loss rate becomes

$$\frac{dM_D}{dt} = 7 \times 10^{21} (\lambda f_\lambda)_{max} \frac{r_A^2 \Delta_A}{\phi_s} \text{ g sec}^{-1}, \qquad (16)$$

where r_A and Δ_A are the heliocentric and geocentric distances in AU, ϕ_s is the beam diameter in arcseconds, and $(\lambda f_\lambda)_{max}$ is the integrated apparent infrared intensity in watts per square centimeter. We emphasize that the mass loss rates calculated above refer only to the emission from the optically important particles. Since a considerable amount of the dust mass is in large particles that do not contribute significantly to the infrared emission (see Jewitt 1991), the mass loss rates given by Eq. (16) are lower limits. Sykes and Walker (1992) suggest that the mass loss in large particles may be more than double that estimated by other means.

The observational results for our sample of comets, normalized to a grain radius of 1 μm, is summarized in Fig. 11, and it is clear from these that the dust mass loss rates for individual comets vary approximately as r_A^{-2}. This heliocentric distance dependency is readily understood by combining Eqs. (11) and (14) to yield:

$$\frac{dM_D}{dt} \propto r_A^{-2}. \qquad (17)$$

Applying Eq. (16) to the data for P/Halley, we find that its average mass loss normalized to a heliocentric distance of 1 AU is $\geq 10^6$ g sec^{-1}. P/Halley's mass loss rate varied

about this mean value by up to a factor of 7 on short time scales (Fig. 11a). For the remaining comets in this study (all IR Type I), Eq. (16) gives a mean loss rate that is a factor of ≈ 10 lower than that for P/Halley (see Fig. 11b). If it is assumed that the IR Type I comets have grains as large as 10 μm, their mass loss rates would be increased by a factor of 10 and would become comparable to the mass loss rate deduced for P/Halley.

IV. CONCLUSIONS

The 0.7- to 23-μm observations reported in this paper for P/Halley and six other bright comets lead to several conclusions about the nature of comet grains and the physics of comet nuclear activity.

(1) Comets can be classified by their thermal infrared energy distributions. IR Type I comets have low continuum superheat and the 10-μm silicate emission is muted or absent. IR Type II comets have large continuum superheat and strong silicate emission features. The differences may be due to grain size.

(2) Simultaneous measurements of P/Halley and Bradfield 1980 XV with different diaphragms using telescopes in Minnesota and Wyoming are generally consistent with the steady-state model for nuclear ablation.

(3) P/Halley's dust coma had an average albedo of 0.20 at a scattering angle of 130°. Our data show that the scattering phase function for typical comet dust is characterized by a moderately strong forward-scattering peak, no appreciable backscattering peak beyond angles of 150°, a mean bolometric albedo of ≈ 0.32, and a sidescattering albedo of ≈ 0.15.

(4) The correlation between superheat and 10-μm silicate excess, the flattened forward-scattering peak of the albedo curve, and the relatively low backscattering albedo are all consistent with laboratory and theoretical results for nonspherical and fluffy grains. These results appear to be especially consistent with core–mantle grain models such as have been proposed by J. M. Greenberg and his collaborators (Greenberg and Hage 1989, Hage and Greenberg 1989).

(5) P/Halley's 10-μm silicate signature showed significant variations in strength and was occasionally weak or absent at heliocentric distances both smaller and larger than 1 AU.

(6) P/Halley's coma luminosity fluctuated by a factor of nearly 10 on time scales of 1 to 2 days. These variations are consistent with the jet-like activity associated with nuclear rotation.

(7) The mass loss rate for P/Halley was highly variable and averaged $\geq 10^6$ g sec^{-1} at $r = 1$ AU. The mass loss rates for the IR Type I comets would be comparable to that deduced for P/Halley if it is assumed that their comae are composed of grains of radius $a \approx 10$ μm.

APPENDIX A: THE STEADY-STATE MODEL FOR INFRARED EMISSION FROM COMA DUST GRAINS

In the so-called "steady-state" model of nuclear activity (see Jewitt 1991), the thermal emission from the coma results from dust grains ablated from the nucleus at a constant rate of dN/dt grains sec^{-1} and flowing away from the nucleus at a constant velocity V_0. Assuming that the coma is optically thin to thermal infrared radiation (see Ney 1982b, Jewitt 1991), the contribution to the apparent infrared intensity of the coma f(IR) by N dust grains is given by

$$f(\mathrm{IR})_{\mathrm{IR}} = \frac{L_{\mathrm{IR}}}{4\pi\Delta^2} = \frac{N 4\pi a^2 Q_e \sigma T_{\mathrm{obs}}^4}{4\pi\Delta^2} = \frac{N a^2 Q_e \sigma T_{\mathrm{obs}}^4}{\Delta^2}, \tag{A-1}$$

where L_{IR} is the coma luminosity, a is the grain radius, Q_e is the Planck mean emission cross section of the grain (Gilman 1974), σ is the Stefan–Boltzmann constant, T_{obs} is the grain temperature, and Δ is the geocentric distance. Assuming that the dust grain distribution is isotropic, the total number of grains in a spherically symmetric coma within a radius r of the nucleus is given by

$$N = 4\pi \int_0^r n(r) r^2 \, dr = \frac{dN}{dt} t = \frac{dN}{dt} \frac{r}{V_0}, \tag{A-2}$$

where $t = r/V_0$ is the time required for grains to flow out to radius r at constant velocity V_0, and $n(r)$ is the radial number density distribution of grains in the coma. Our multiaperture measurements typically occurred when Δ was between 1 and 1.5 AU, so that the residence time of grains with $V_0 = 0.5$ km sec^{-1} in the beams we used was between 0.6 hr (2.2-arcsec beam) and 6 hr (20-arcsec beam). By inspection of Eq. (A-2), it follows that the steady-state model leads to a radial grain density distribution in the coma of

$$n(r) = \frac{1}{4\pi r^2 V_0} \frac{dN}{dt}. \tag{A-3}$$

Integrating this density distribution over the cylindrical volume V of the coma that is intercepted by a photometer beam of angular diameter ϕ to obtain the number N_ϕ of grains emitted into the beam, and substituting the result into Eq. (A-1), we find that the apparent infrared intensity ℓ_ϕ(IR) measured in the beam is

$$f_\phi(\mathrm{IR}) = \frac{a^2 Q_e \sigma T_{\mathrm{obs}}^4}{\Delta^2} N_\phi = \frac{a^2 Q_e \sigma T_{\mathrm{obs}}^4}{\Delta^2} \int\int\int_V n(r) \, d^3 r = \left[\frac{\pi a^2 Q_e \sigma T_{\mathrm{obs}}^4}{4 V_0}\right] \frac{\phi}{\Delta} \frac{dN}{dt}, \tag{A-4}$$

where the result on the extreme right-hand side is for the case where the angular diameter of the beam is much smaller than the angular diameter of the coma. It can be seen from Eq. (A-2) that $f_\phi(\mathrm{IR}) \propto \phi\Delta^{-1}$, leading to the correction terms specified in Eqs. (B-1) and (B-2) that we derive in Appendix B.

The determination of f_ϕ(IR) is particularly straightforward when the continuum emission from the dust approximates that of a blackbody as is the case with all the comets observed here. In this case, the ratio of the maximum of the λF_λ function to the total blackbody emission F is given by

TABLE C-I
Orbital Elements for the Comets

COMET	KBM 1975 IX	Bradfield 1980 XV	Austin 1984 XIII	Machholz 1985 VIII	Austin 1989c$_1$	BM 1989X	P/Halley 1986 III
EQUINOX	1950.0	1950.0	1950.0	1950.0	J2000.0	J2000.0	J2000.0
EPOCH	5 Sep 25	80 Dec 27	84 Aug 8	-	90 Apr 19	89 Oct 1	86 Feb 19
T	75 Sep 5.3348	80 Dec 29.5417	84 Aug 12.1371	85 Jun 28.7388	90 Apr 9.96745	89 Sep 11.9384	86 Feb 9.4590
q	0.425561	0.259823	0.291284	0.106252	0.349775	0.478742	0.587104
e	1.000095	0.999725	0.999846	1.000000	1.000225	0.971959	0.967277
P	-	-	-	-	-	-	76.00
PERI (ω)	116.9756	358.2855	353.12701	274.0831	61.5763	129.6111	111.8657
NODE (Ω)	295.6526	114.6465	170.87724	194.7292	75.9255	311.5878	58.8601
INCL (i)	80.7779	138.5882	164.15979	16.2827	58.95639	19.3357	162.2422

$$\frac{(\lambda F_\lambda)_{\max}}{F} = \frac{2\pi hc^2}{\sigma(\lambda_m T)^4}\left[\frac{1}{e^{hc/k(\lambda_m T)} - 1}\right] = \frac{1}{1.3586}, \tag{A-5}$$

where λ_m is the wavelength of maximum emission in λF_λ, $\lambda_m T = 0.3670$ cm deg is Wien's law for λF_λ, $h = 6.6262 \times 10^{-27}$ erg sec, $c = 2.9979 \times 10^{10}$ cm sec^{-1}, $\sigma = 5.6696 \times 10^{-5}$ erg cm^{-2} deg^{-4} sec^{-1} and $k = 1.3806 \times 10^{-16}$ erg deg^{-1}. Thus, the apparent infrared intensity f_ϕ(IR) of the coma is given by

$$f_\phi(\mathrm{IR}) = 1.3586(\lambda f_\lambda)_{\max}, \tag{A-6}$$

where $(\lambda f_\lambda)_{\max}$ is the observed apparent emission maximum of the infrared continuum.

APPENDIX B: CORRECTIONS FOR BEAM DIAMETER, THROW, AND GEOCENTRIC DISTANCE

Comet comae are extended sources of infrared emission and are large enough so that coma emission is present in the reference beam used for background cancellation. The total emission into a beam of a given angular diameter depends upon the volume of coma material intercepted by the beam. Therefore, analysis and interpretation of the infrared photometry require correction of the data for the effects of beam diameter, reference beam throw, and geocentric distance. The correction is straightforward for comets that obey a steady-state model where the coma is produced by material ablated from the nucleus at a constant rate and flowing away from the nucleus at a constant velocity. We describe this model quantitatively in Appendix A, concluding that it leads to a ϕ^{+1} dependence for the flux from the coma, where ϕ is the radius of the coma, and a Δ^{-1} dependence of the coma brightness on geocentric distance. In this case, the apparent intensity f_∞ that would be measured in a beam of angular diameter ϕ for a throw large enough so that the reference beam falls off the coma and the apparent intensity f_ψ observed in the same beam with a throw of angular diameter ψ such that the reference beam falls on the coma are related by

$$\frac{f_\infty}{f_\psi} = \frac{4\psi}{4\psi - \phi}. \tag{B-1}$$

Furthermore, the apparent intensities, f_1 and f_2 measured in two different apertures with diameters ϕ_1 and ϕ_2 with the comet at geocentric distances of Δ_1 and Δ_2, respectively, will be related by

$$\frac{f_1}{f_2} = \frac{\phi_1\Delta_2}{\phi_2\Delta_1}. \tag{B-2}$$

These correction factors have been applied where appropriate in the analysis above using a standard reference beam diameter of $\phi_1 = 20$ arcsec and a standard geocentric distance of $\Delta_1 = 1$ AU.

APPENDIX C: ORBITAL ELEMENTS FOR THE COMETS OBSERVED

We present in Table C-I the orbital elements we used for deriving the orbital parameters of the comets for which we report infrared observations here. These have been gleaned from the *Catalog of Cometary Orbits* (Marsden 1982) and The Central Bureau for Astronomical Telegrams (Marsden 1992). The data tabulated by row are (1) the comet name, (2) the equinox for Ω, ω, and the orbital inclination (i), (3) the osculation date in decimal days (Universal, or Ephemeris, Time), (4) the perihelion time (Ephemeris Time), (5) the perihelion distance q in astronomical units, (6) the orbital eccentricity, (7) the revolution period in years (no entry signifies $p > 1000$ years), (8) the argument of perihelion ω in decimal degrees, (9) the longitude of the ascending node Ω in decimal degrees, and (10) the orbital inclination i in decimal degrees.

ACKNOWLEDGMENTS

We are especially grateful to D. Hufmann for giving freely of his time to discuss with us the characteristics of the phase function of comet dust particles; his comments weighed heavily in the framing of our conclusions. M. S. Hanner helpfully provided us with her insightful lecture notes on defining albedos for small particles, and T. J. Jones gave us guidance on the definition of albedos. T. W. Jones confirmed the conversion factors between square and circular apertures for an r^{-1} surface brightness distribution. We thank B. Jones for a critical reading of the manuscript and for suggesting several improvements in the presentation. T. Williams, L. R. Shaw, T. Hayward, C. Jaworosky, and L. Chisholm assisted with the observations at WIRO. Hayward's contributions were especially valuable and included a crucial last-minute repair of the photometer at WIRO during the remote observations of P/Halley on perihelion day. He also obtained the 15.79 April 1990 UT observation of Comet Austin 1989c$_1$ for us at WIRO. A. Knutson provided invaluable assistance with observations at O'Brien Observatory. We thank T. J. Jones for obtaining the 27.3 and 28.3 April 1986 UT observations of P/Halley at MLOF for us. Finally, A. Tokunaga and A. Storrs, who

refereed the manuscript, made several useful suggestions that improved the clarity of the presentation. This research was supported by NASA, the National Science Foundation, the U.S. Air Force, and the University of Minnesota Institute of Technology Dean's Office and Graduate School, and the University of Wyoming.

REFERENCES

BECKLIN, E. E., AND J. A. WESTPHAL 1966. Infrared observations of comet 1965f. *Astrophys. J.* **145,** 445–453.

BOHREN, C. F., AND D. R. HUFMANN 1983. *Absorption and Scattering of Light by Small Particles,* pp. 399–401. Wiley, New York.

BREGER, M., R. D. GEHRZ, AND J. A. HACKWELL 1981. Interstellar grain size. II. Infrared photometry and polarization in Orion. *Astrophys. J.* **248,** 963–976.

BROOKE, T. Y., R. F. KNACKE, AND R. R. JOYCE 1986. Near-infrared studies of comet Halley: polarization and color. In *Exploration of Halley's Comet,* ESA SP-250, pp. 87–89. European Space Agency, Noordwijk.

BROOKE, T. Y., R. F. KNACKE, T. C. OWEN, AND A. T. TOKUNAGA 1988. Spectroscopy of emission features near 3 μm in comet Wilson (1986l), submitted for publication.

BROOKE, T. Y., A. T. TOKUNAGA, AND R. F. KNACKE 1991. Detection of the 3.4 μm emission feature in comets P/Brorson–Metcalf and Okazaki-Levy-Rudenko (1989R) and an observational summary. *Astron. J.* **101,** 268–278.

BROWNLEE, D. E. 1987. A comparison of Halley dust with meteorites, interplanetary dust, and interstellar grains. In *Observations of Comets Halley and Wilson and Properties of the Grains,* (M. Hanner, Ed.), NASA Conference Publ. 3004, pp. 66–67.

BROWNLEE, D. E., L. PILACHOWSKI, E. OLSZEWSKI, AND P. W. HODGE 1980. Analysis of interplanetary dust collections. In *Solid Particles in the Solar System* (I. Halliday and B. A. McIntosh, Eds.), pp. 333–342. Reidel, Dordrecht.

CASTELAZ, M. W., J. A. HACKWELL, G. L. GRASDALEN, R. D. GEHRZ, AND C. GULLIXSON 1985. GSS 30: an infrared reflection nebula in the Ophiuchus dark cloud. *Astrophys. J.* **290,** 261–272.

EATON, N. 1984. Comet dust—Applications of Mie scattering. *Vistas Astron.* **27,** 111–129.

FINSON, M. L., AND R. F. PROBSTEIN 1968. A theory of dust comets: I. Model and equations and II. Results for Comet Arend–Roland. *Astrophys. J.* **154,** 327.

FRAUNDORF, P., D. E. BROWNLEE, AND R. M. WALKER 1982. Laboratory studies of interplanetary dust. In *Comets,* (L. Wilkening, Ed.), pp. 323–340. Univ. of Arizona Press, Tucson.

GEHRZ, R. D., AND J. A. HACKWELL 1978. Exploring the infrared universe from Wyoming. *Sky Telescope* **55,** 466–473.

GEHRZ, R. D., AND E. P. NEY 1986. Infrared temporal development of P/Halley. In *Exploration of Halley's Comet,* ESA SP-250, pp. 101–105. European Space Agency, Noordwijk.

GEHRZ, R. D., G. L. GRASDALEN, AND J. A. HACKWELL 1987. Infrared astronomy. In *Encyclopedia of Physical Science and Technology,* Vol. 2, pp. 53–80. Academic Press, New York.

GEHRZ, R. D., J. A. HACKWELL, AND T. W. JONES 1974. Infrared observations of Be stars from 2.3 to 19.5 microns. *Astrophys. J.* **191,** 675–684.

GEHRZ, R. D., E. P. NEY, J. PISCATELLI, E. ROSENTHAL, AND A. T. TOKUNAGA 1989. Infrared photometry and spectroscopy of Comet P/Encke 1987. *Icarus* **80,** 280–288.

GILMAN, R. C. 1974. Planck mean cross-sections for four grain materials. *Astrophys. J. Suppl. Ser.* **28,** 397–403.

GREEN, D. W. E., AND C. S. MORRIS 1987. The visual brightness behavior of P/Halley during 1981–1987. *Astron. Astrophys.* **187,** 560–568.

GREENBERG, J. M. 1982. In *Comets* (L. L. Wilkening, Ed.), pp. 131–163. Univ. of Arizona Press, Tucson.

GREENBERG, J. M. 1986. Predicting that comet Halley is dark. *Nature* **321,** 385.

GREENBERG, J. M., AND J. I. HAGE 1990. From interstellar dust to comets: A unification of observational constraints. *Astrophys. J.* **361,** 260–274.

HAGE, J. I., AND J. M. GREENBERG 1990. A model for the optical properties of porous grains. *Astrophys. J.* **361,** 251–259.

HANNER, M. S. 1988. Grain optical properties. In *Observations of Comets Halley and Wilson and Properties of the Grains* (M. S. Hanner, Ed.), pp. 22–49. NASA Conference Publ. 3004.

HANNER, M. S., R. H. GIESE, K. WEISS, AND R. ZERULL 1981. On the definition of albedo and application to irregular particles. *Astron. Astrophys.* **104,** 42–46.

HANNER, M. S., D. K. AITKEN, R. KNACKE, S. MCCORKLE, P. F. ROCHE, AND A. T. TOKUNAGA 1985a. Infrared spectrophotometry of Comet IRAS–Araki–Alcock (1983d): A bare nucleus revealed? *Icarus* **62,** 97–109.

HANNER, M. S., R. KNACKE, Z. SEKANINA, AND A. T. TOKUNAGA 1985b. Dark grains in Comet Crommelin. *Astron. Astrophys.* **152,** 177–181.

HANNER, M. S., E. TEDESCO, A. T. TOKUNAGA, G. J. VEEDER, D. F. LESTER, F. C. WITTEBORN, J. D. BREGMAN, J. GRADIE, AND L. LEBOFSKY 1985c. The dust coma of periodic Comet Churyumov–Gerasimenko (1982 VIII). *Icarus* **64,** 11–19.

HANNER, M. S., A. T. TOKUNAGA, W. F. GOLISCH, D. M. GRIEP, AND C. D. KAMINSKI 1987. Infrared emission from P/Halley's dust coma during March 1986. *Astron. Astrophys.* **187,** 653–660.

HANNER, M. S., R. L. NEWBURN, R. D. GEHRZ, A. T. HARRISON, AND E. P. NEY 1990. The infrared spectrum of comet Bradfield (1987s) and the silicate emission feature. *Astrophys. J.* **348,** 312–321.

HAYWARD, T., R. D. GEHRZ, AND G. L. GRASDALEN 1986. Ground-based infrared observations of comet Halley. *Nature* **326,** 55–57.

JEWITT, D. 1991. Cometary photometry. In *Comets in the Post-Halley Era* (R. L. Newburn, Jr., M. Neugebauer, and J. Rahe, Eds.), Vol. 1, pp. 19–64. Kluwer, Dordrecht.

JEWITT, D., AND K. J. MEECH 1986. Cometary grain scattering versus wavelength, or, "What color is comet dust?" *Astrophys. J.* **310,** 937–952.

KELLER, H. U., *et al.* 1986. First Halley multicolor camera imaging results from Giotto. *Nature* **321,** 320–326.

KISSEL, J., *et al.* 1986. Composition of comet Halley dust particles from Giotto observations. *Nature* **321,** 336–337.

MAAS, R. W., E. P. NEY, AND N. J. WOOLF 1970. The 10 micron emission peak of comet Bennett 1969i. *Astrophys. J.* **160,** L101–L104.

MARSDEN, B. G. 1982. *Catalog of Cometary Orbits,* 4th ed. Minor Planet Center, Smithsonian Astrophysical Observatory, Cambridge, MA.

MARSDEN, B. G. 1992. *IAU Circulars, e-mail service.*

MCDONNELL, J. A. M., *et al.* 1987. The dust distribution within the inner coma of comet P/Halley 1982i: Encounter by *Giotto*'s impact detectors. *Astron. Astrophys.* **187,** 719–741.

MCDONNELL, J. A. M., P. L. LAMY, AND G. S. PANKIEWICZ 1991. Physical properties of cometary dust. In *Comets in the Post-Halley Era* (R. L. Newburn, Jr., M. Neugebauer, and J. Rahe, Eds.), Vol. 2, pp. 1043–1073. Kluwer, Dordrecht.

MCFADDEN, L. A., M. F. A'HEARN, P. D. FELDMAN, E. E. ROETTGER, D. M. EDSALL, AND P. S. BUTTERWORTH 1987. Activity of Comet

P/Halley 23–25 March, 1986: IUE observations. *Astron. Astrophys.* **187,** 333–338.

MILLIS, R. L., AND D. G. SCHLEICHER 1986. Rotational period of comet Halley. *Nature* **324,** 646–649.

NEY, E. P. 1974a. Infrared observations of comet Kohoutek near perihelion. *Astrophys. J.* **189,** L141–L143.

NEY, E. P. 1974b. Multiband photometry of comets Kohoutek, Bennett, Bradfield, and Encke. *Icarus* **23,** 551–560.

NEY, E. P. 1977. Star Dust. *Science* **195,** 541–546.

NEY, E. P. 1982a. Optical and infrared observations of bright comets in the range 0.5 μm to 20 μm. In *Comets* (L. Wilkening, Ed.), pp. 323–340. Univ. of Arizona Press, Tucson.

NEY, E. P. 1982b. Visibility of comet nuclei. *Science* **215,** 397–398.

NEY, E. P., AND K. M. MERRILL 1976. Comet West and the scattering function of cometary dust. *Science* **194,** 1051–1053.

REITSEMA, H. J., W. A. DELAMERE, A. R. WILLIAMS, D. C. BOICE, W. F. HUEBNER, AND F. L. WHIPPLE 1989. Dust distribution in the inner coma of Comet Halley: Comparison with models. *Icarus* **81,** 31–40 (see also the cover illustration of *Planetary Rep.* **VII**(5), Sept./Oct. 1987).

RETTIG, T. W., J. R. KERN, R. RUCHTI, B. BAUMBAUGH, A. E. BAUMBAUGH, K. L. KNICKERBOCKER, AND J. DAWE 1987. Observations of the coma of Comet P/Halley and the outburst of 1986 March 24–25 (UT). *Astron. Astrophys.* **187,** 249–255.

RIEKE, G. H., F. J. LOW, T. A. LEE, AND W. W. WISNIEWSKI 1974. Infrared observations of comet Kohoutek. In *Comet Kohoutek,* NASA-SP 355, pp. 175–182. NASA, Washington DC.

ROSE, L. A. 1979. Laboratory simulation of infrared astrophysical features. *Astrophys. Space Sci.* **65,** 47–67.

RYAN, E. V., AND H. CAMPINS 1991. Comet Halley: Spatial and temporal variability of the silicate emission feature. *Astron. J.* **101,** 695–705.

SCHLEICHER, D. G., R. L. MILLIS, D. T. THOMPSON, P. V. BIRCH, R. MARTIN, D. J. THOLEN, J. R. PISCITELLI, N. L. LARK, AND H. B. HAMMEL 1990. Periodic variations in the activity of comet P/Halley during the 1985/1986 apparition. *Astron. J.* **100,** 896–912.

SEKANINA, Z. 1974a. On the nature of the anti-tail of Comet Kohoutek (1973f) I. a working model. *Icarus* **23,** 502–518.

SEKANINA, Z. 1974b. The prediction of anomalous tails of comets. *Sky Telescope* **47,** 374–377.

SEKANINA, Z. 1976. In *The Study of Comets* (B. Donn, M. Mumma, W. Jackson, M. A'Hearn, and R. Harrington, Eds.), NASA SP-393, pp. 893–933. U.S. G.P.O., Washington, D.C.

SYKES, M. V., L. A. LEBOFSKY, D. M. HUNTEN, AND F. LOW 1986. The discovery of dust trails in the orbits of periodic comets. *Science* **232,** 1115–1117.

SYKES, M. V., AND R. G. WALKER 1992. Cometary dust trails. *Icarus* **95,** 180–210.

TELESCO, C. M., R. DECHER, C. BAUGHER, H. CAMPINS, D. MOZURKEWICH, H. A. THRONSON, D. P. CRUIKSHANK, H. B. HAMEL, S. LARSON, AND Z. SEKANINA 1986. Thermal-infrared and visual imaging of comet Giacobini-Zinner. *Astrophys. J.* **310,** L61–L65.

TEMI, P., P. DE BERNARDS, S. MASI, G. MORENO, AND A. SALAMA 1989. Infrared emission from interplanetary dust. *Astrophys. J.* **337,** 528–535.

TOKUNAGA, A. T., W. F. GOLISCH, D. M. GRIEP, C. D. KAMINSKI, AND M. S. HANNER 1986. The NASA Infrared Telescope Facility comet Halley monitoring program. I. Preperihelion results. *Astron. J.* **92,** 1183–1190.

TOKUNAGA, A. T., W. F. GOLISCH, D. M. GRIEP, C. D. KAMINSKI, AND M. S. HANNER 1988. The NASA Infrared Telescope Facility comet Halley monitoring program. II. Postperihelion results. *Astron. J.* **96,** 1971–1976.

VAN DE HULST, H. C. 1957. *Light Scattering by Small Particles,* pp. 183 and 449. Dover, New York.

WALKER, R. M. 1987. Comparison of laboratory determined properties of interplanetary dust with those of comet Halley particles: What are comets made of? In *Infrared Observations of Comets Halley and Wilson and Properties of the Grains* (M. Hanner, Ed.), NASA Conference Publ. 3004, pp. 53–63.

WEAVER, H. A., M. F. A'HEARN, P. D. FELDMAN, C. ARPIGNY, W. A. BAUM, J. C. BRANDT, R. M. LIGHT, AND J. A. WESTPHAL 1992. Inner coma imaging of Comet Levy (1990C) with the Hubble Space Telescope. *Icarus,* in press.

WEBB, C. G. 1935. The scattering of light by drops in a Wilson chamber. *Philos. Mag.* **19,** 927–933.

WILSON, J. G. 1951. *The Principles of Cloud-Chamber Technique,* p. 59. Cambridge Univ. Press, Cambridge.

WOOLF, N. J., AND E. P. NEY 1969. Circumstellar emission from cool stars. *Astrophys. J.* **155,** L181–L184.